FACULDADE DE ENGENHARIA DA UNIVERSIDADE DO PORTO

Guidance of an Autonomous Surface Vehicle for Underwater Navigation Aid

José Pedro Martins Pires e Sousa

Mestrado Integrado em Engenharia Eletrotécnica e de Computadores

Supervisor: Nuno Alexandre Cruz

Co-Supervisor: Bruno Mateus Ferreira

July 20, 2018

Resumo

Veículos Submarinos não Tripulados (UUVs), tais como Veículos Submarinos Autónomos (AUVs) e Veículos de Controlo Remoto (ROVs) são ferramentas versáteis, adequadas a diversas atividades para diferentes áreas, e tem vindo a registar um aumento de uso, fazendo das mesmas uma área de interesse no estudo da robótica.

Em termos gerais, a performance de qualquer veículo submarino em qualquer tarefa é profundamente afetada pela precisão do seu sistema de localização. O principal desafio da localização submarina é a atenuação significativa de qualquer sinal submarino de frequência de radio (RF) que impede o uso dos métodos de localização habitualmente usados tais como Sistema de Posicionamento Global (GPS). Muitos métodos foram estudados para a localização de UUVs, incluindo o uso de faróis acústicos. Um destes métodos é o uso de um único farol móvel para obter alcances acústicos, ao contrário de um farol imóvel, que restringe a trajetória dos UUVs, ou múltiplos faróis que envolvem mais hardware, complicando a logística das missões e um aumento dos custos.

Nesta dissertação é proposto um algoritmo de navegação com base na Matriz de Informação de Fisher para um veículo de superfície autónomo que tem como função ajudar na navegação de um veiculo subaquático.

Abstract

Unmanned Underwater Vehicles (UUVs), such as Autonomous Underwater Vehicles (AUVs) and Remote Operated Vehicles (ROVs) are versatile tools, suitable for many activities in different fields, and have seen an increase in usage, making them an area of interest in the study of robotics.

Generically speaking, the performance of any underwater vehicle in any given task is deeply affected by the precision of its localization system. The main challenge in underwater localization is the significant attenuation of any Radio Frequency (RF) signal underwater, which prevents the use of many common location methods such as the Global Positioning System (GPS). Many methods have been studied for the localization of UUVs, including the use of acoustic beacons. One of these methods is the use of a single moving beacon to obtain acoustic ranges, as opposed to a stationary single beacon, which restricts the UUV's trajectory or multiple beacons, which involve more hardware, complicating missions' logistics and increasing costs.

In this dissertation a guidance algorithm based on the Fisher Information Matrix is proposed for an Autonomous Surface Vehicle to serve as a beacon vehicle and aid in the navigation of a UUV.

Ackowledgements

Em primeiro lugar gostaria de agradecer ao professor Nuno Cruz e ao professor Bruno Ferreira por todo o tempo dedicado e disponibilidade que demonstraram ao longo desta dissertação. Em último. mas não menos importante, à minha família, amigos e colegas de curso que decerto compreendem o porquê desta brevidade no agradecimento.

'Obrigades'

José Pedro Martins Pires e Sousa

“One man’s ’magic’ is another man’s engineering."

Robert Heinlein

Contents

List of Figures

List of Tables

Acronyms

ASV	Autonomous Surface Vehicle
AUV	Autonomous Underwater Vehicle
CN	Cooperative Navigation
CNA	Communication and Navigation Aid
CRLB	Cramer-Rao Lower Bound
DOF	Degrees of Fredom
DR	Dead Reckoning
DVL	Doppler Velocity Log
EKF	Extended Kalman Filter
FIM	Fisher Information Martix
GPS	Global Positioning System
KF	Kalman Filter
LBL	Long Baseline
NED	North East Down
OWTT	One-Way Travel Time
PF	Particle Filter
RF	Radio Frequency
ROV	Remote Operated Vehicle
SBL	Short Baseline
TOT	Time of Travel
TWTT	Two-Way Travel Time
USBL	Ultra Short Baseline
UUV	Unmanned Underwater Vehicle

Chapter 1

Introduction

1.1 Context and Motivation

Unmanned Underwater Vehicles (UUVs), such as Autonomous Underwater Vehicles (AUVs) and Remote Operated Vehicles (ROVs) are versatile tools, suitable for many activities in different fields. Besides the obvious scientific interest in ocean exploration by itself, UUVs can be useful in industrial applications such as monitoring underwater pipelines and communication lines and may also be used for military purposes. Even though their main advantage is avoiding risk to human lives, they also allow the simplification of missions' logistics and the reduction of their costs.

The performance of any underwater vehicle in any given task is deeply affected by the precision of its localization system. The main challenge in underwater localization is the significant attenuation of any Radio Frequency (RF) signal underwater, which prevents the use of many common location methods such as the Global Positioning System (GPS). In order to overcome this difficulty, multiple localization techniques have been developed, based on different technologies.

To increase the number of potential UUV applications, continued development and improvement of every subsystem is needed. The aforementioned localization system is one with much room for improvement, with new solutions frequently arising.

Cooperative Navigation (CN) is one of these solutions. In CN, a UUV determines its position relatively to another vehicle that can determine its own position with certainty, like a surface vehicle equipped with GPS. This vehicle is called a Communication and Navigation Aid (CNA) vehicle. CN localization methods using only one support vehicle are appealing, to lower costs and logistics, but they require good positioning of the CNA vehicle to maintain observability and achieve good performances.

1.2 Objective

The purpose of this dissertation is to develop a navigation system for a CNA surface vehicle. In a CN localization system, the UUV estimates its own pose with Dead Reckoning (DR) techniques and periodically obtains ranges from CNA vehicles to improve this estimate. The direction of the

obtained ranges is particularly important, hence the need to adapt the surface vehicle's trajectory to the requirements of the UUV. The navigation system developed should be able to determine in real time the trajectory of the CNA that minimizes the position uncertainty of the UUV.

Chapter 2

State of the Art

2.1 Underwater Vehicle Localization

As mentioned in chapter 1, the accuracy of localization systems is a crucial factor in the performance of underwater vehicles. As opposed to the localization of surface vehicles, where the position can obtained using GPS based systems, there are many challenges in underwater localization. On the one hand, the significant attenuation of any electromagnetic signals [1] renders the use of GPS and other RF based techniques infeasible.

On the other hand, acoustic based communications are not as attenuated by water, but they have many restraints in bandwidth, data rate and reliability, caused by low and variable sound speed in water and multi-path transmissions, caused by sound reflection on the sea surface and floor [2]. Considering these technological and physical restrictions many localization methods were developed. Figure 2.1 shows an overview of used underwater localization methods and used technologies. These are usually combined to obtain precise localization systems.

As stated in [2], underwater localization methods can be divided in three main categories, which are listed below.

- Dead reckoning/inertial: uses the vehicle's motion state and previous position to determine the current pose.
- Acoustic: Uses the time of flight of an acoustic signal between the vehicle and one or more beacons to determine localization.
- Geophysical: Uses know features of the environment to determine position. This can be accomplished, for example, with artificial vision or sonars.

2.1.1 Dead-reckoning

As mentioned before, DR localization methods use the knowledge of the vehicle's previous location, as well as its current speed (obtained from a Doppler Velocity Log (DVL), for example) and orientation to determine the current pose. Inertial systems improve the DR estimation using information from gyroscopes and accelerometers. Since the depth of underwater vehicles can

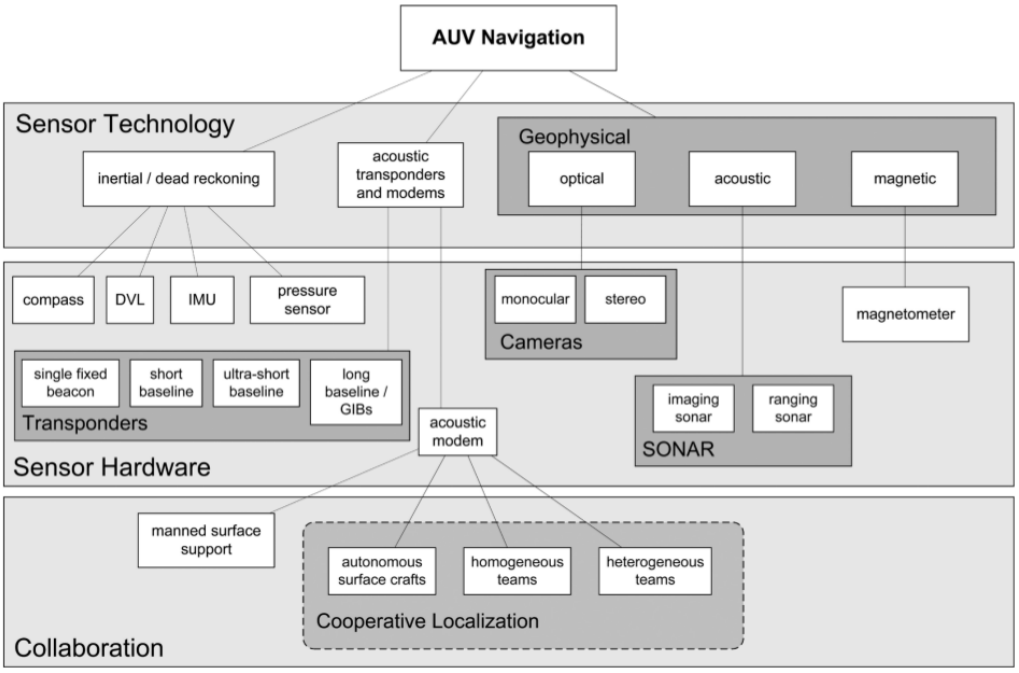

Figure 2.1: Overview of underwater location methods and classifications [2].

be determined precisely using pressure sensors [2], underwater localization solutions are usually focused on the horizontal plane.

The main issue with this method is that its errors are cumulative, leading to unbounded position error growth with time and distance. Figure 2.2 shows an example of growth in position error of a vehicle traveling along the X axis. The uncertainty in velocity is predominant in the error growth in the movement direction, while the error in the direction perpendicular to movement is mostly affected by heading uncertainty [1].

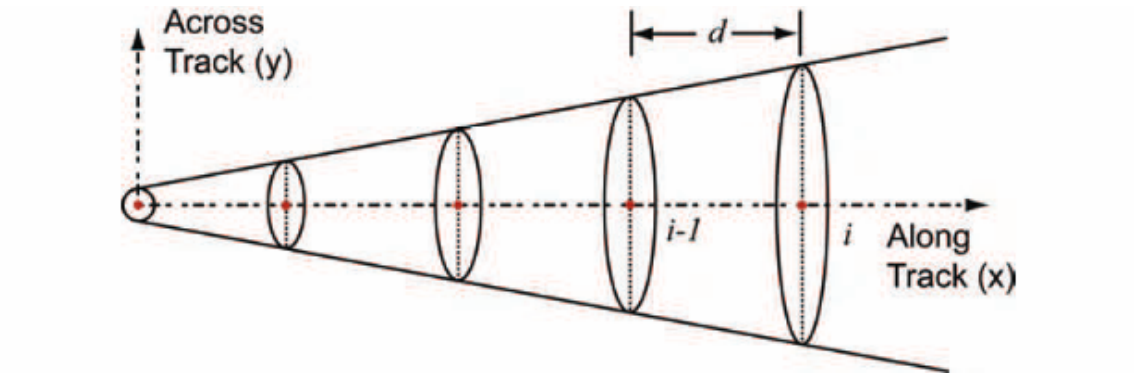

Figure 2.2: Example error growth in Dead Reckoning [1].

2.1.2 Acoustic Localization

Acoustic localization of an object is based on measuring the Time of Travel (TOT) of acoustic signals between the vehicle and acoustic beacons to determine the distance between them. These ranges can be obtained using One-Way Travel Time (OWTT) of a signal sent by the beacon to the vehicle (or vice-versa) or Two-Way Travel Time (TWTT) of a signal sent round-trip between them. Synchronization between the beacon and vehicle is required to use OWTT to determine the range.

There are many methods that use acoustic signals to determine the position of a UUV which are characterized by the baseline length and number and type of modems used [3]. Some methods, such as Long Baseline (LBL), Short Baseline (SBL) and Ultra Short Baseline (USBL) use multiple beacons to measure distances and or directions of the object being tracked, as shown in figure 2.3.

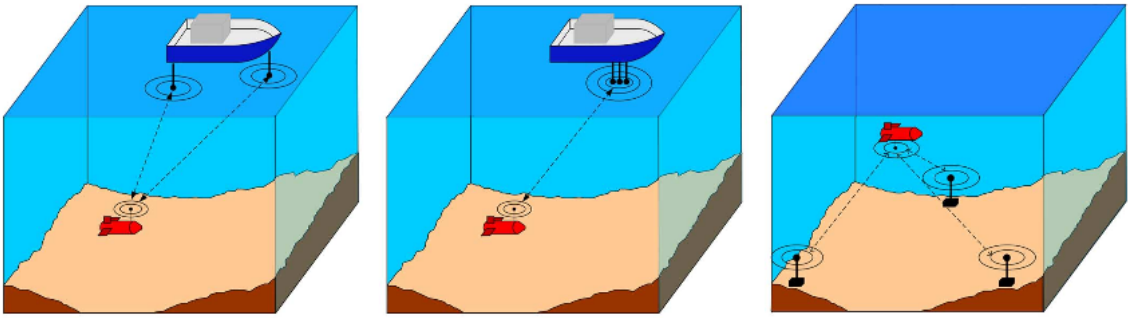

Figure 2.3: Example of SBL, USBL and LBL localization methods [2].

The main difference between the aforementioned systems is the baseline length. LBL systems usually have a baseline length of 50-2000 m, while the baseline length of a SBL system is typically between 20-50 m. Transceivers in an USBL system are usually less than 10 cm apart [3]. Another key difference between these systems is the use of trilateration to determine the object's position in LBL and SBL systems, while USBL uses the object's distance and angle to determine the vehicles localization.

While the previously mentioned methods allow unambiguous location of UUVs, they do so at a cost. On the one hand all of them require the use of multiple transponders, increasing the cost of the system. On top of that, LBL systems also require the deployment of an infrastructure in the area of interest prior to any mission, which complicates logistics. Single beacon approaches are commonly used to reduce these demands. In these systems location is determined by combining received ranges with DR. As seen in figure 2.4, uncertainty is reduced upon beacon updates, and is increased between these. Upon updates from the acoustic beacon, the reduction of uncertainty is always in the direction of the mentioned beacon. [2].

The main shortcoming of this approach is that its performance depends on the vehicle's trajectory [2], since long paths away from or towards the beacon result in unbounded position error growth. However, certain studies relating the trajectory of the vehicle to the observability of the system [4] and derive conditions of observability for the system in single range navigation [5].

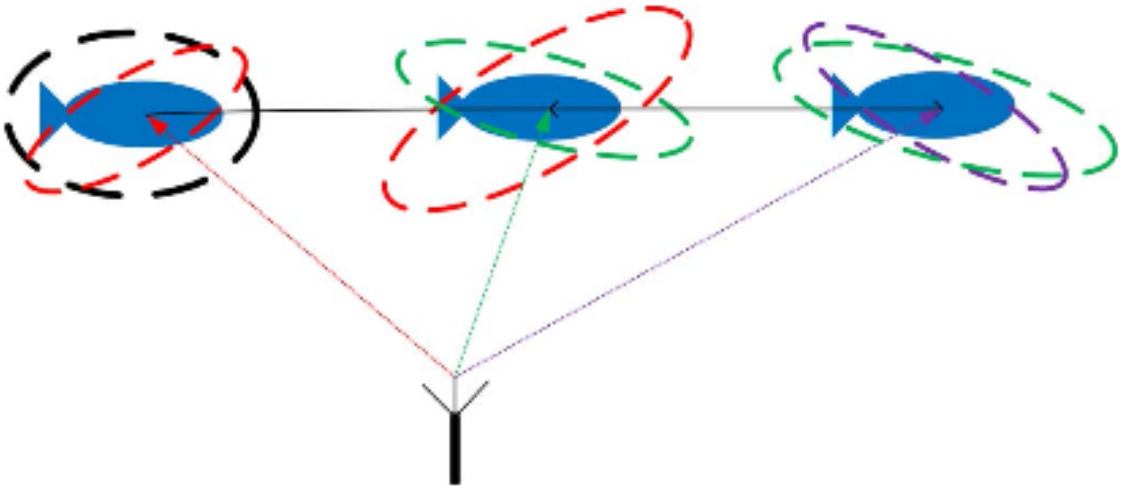

Figure 2.4: Uncertainty variation between updates in single beacon system [2].

One way to overcome this problem is having a transponder attached to a vehicle with the ability of determining its position with minimal uncertainty so that other vehicles can use it as a beacon for localization purposes. This vehicle is referred to as master vehicle, CNA vehicle or beacon vehicle [6]. This method is commonly referred to as CN. CNA vehicles can either be underwater vehicles, as in [7] or surface vehicles, as seen in [8] and also in [9].

Recent works in CN, such as [7] and [10], focus on path planning of the beacon vehicle, since it is one of the most determining aspects in state observability and uncertainty. Tracking underwater objects with range measurements alone has also been studied in [11].

2.2 Marine Vehicle Modelling

In order to develop work regarding any vehicle it is important to understand the dynamics of the vehicle. As explained in [12], there are two parts of the study of dynamics: kinematics, which deals with the geometrical aspects of motion and kinetics, the analysis of the underlying forces. In this dissertation only the kinematics are taken into account.

In this dissertation two reference frames are used as described in[12]: the North East Down (NED) frame {n}, defined as the tangent plane on the surface of the Earth moving with the craft with the x axis pointing towards the true North, the y axis pointing East and the z axis pointing downwards normal to the sea surface and the body-fixed reference frame {b}, a moving coordinate frame fixed to the craft.

The UUV is assumed to be a vehicle with 6 Degrees of Fredom (DOF) and the vectorial notation used in this dissertation is the following [12]:

- NED position $p = \begin{bmatrix} N \\ E \\ D \end{bmatrix}$
- Attitude (Euler Angles between {b} and {n}) $\Theta_{bn} = \begin{bmatrix} \phi \\ \theta \\ \psi \end{bmatrix}$
- Body-fixed linear velocity $\nu^b_{b/n} = \begin{bmatrix} u \\ v \\ w \end{bmatrix}$
- Body-fixed angular velocity $\omega^b_{b/n} = \begin{bmatrix} p \\ q \\ r \end{bmatrix}$

Using the above vectors, the two vectors shown in (2.1) are used to characterize the motion of the UUV, where X describes the position and attitude of the vehicle and ν describes its angular and linear velocities.

$$X = \begin{bmatrix} p \\ \Theta \end{bmatrix} \quad \nu = \begin{bmatrix} \nu^b_{b/n} \\ \omega^b_{b/n} \end{bmatrix} \tag{2.1}$$

The surface vehicle is assumed to be a vehicle with 3 DOF, so a simplification of (2.1) is used to describe its motion. The vectors that characterize the surface vehicles motion are shown in 2.2.

$$X = \begin{bmatrix} N \\ E \\ \psi \end{bmatrix} \quad \nu = \begin{bmatrix} u \\ v \\ r \end{bmatrix} \tag{2.2}$$

2.3 Tools and methods

2.3.1 Filters

When developing localization systems like the ones mentioned above, it is important to have an appropriate method to deal with uncertainty in measurements and position, as well as merge information obtained from different sources. Two alternatives are presented, the Kalman Filter and the Particle Filter.

As explained in [13], the Kalman Filter (KF) is a technique for filtering and prediction in linear systems. In a Kalman Filter a belief is represented at each moment t by a Gaussian distribution with mean μ_k and covariance Σ_k. In the Kalman Filter the state transition is assumed to be linear Gaussian *i.e.*, linear with additive Gaussian noise of zero mean and covariance R_t. The measurements are also assumed to be linear, with added Gaussian noise of zero mean and covariance Q_t.

In each iteration of the KF algorithm a belief is predicted using the previous belief and the transition model. This causes an increase in uncertainty, due to the stochastic nature of the state transition. If measurements are available, the current belief is updated with this information. The update phase decreases the belief's uncertainty. An example of the KF algorithm for a one-dimensional scenario is shown in figure 2.5, where robot location belief, as well as measurements are displayed as normal distributions. The example shows different steps in time, as follows.

a. The initial belief is shown.

b. In this step, a measurement has been obtained and is represented by the bold line.

c. A third line is shown, corresponding to the updated belief, after integrating the measurement into the initial one.

d. The line on the right is the predicted belief after the robot moves to the right.

e. Again, a new measurement is obtained.

f. The measurement is integrated into the belief.

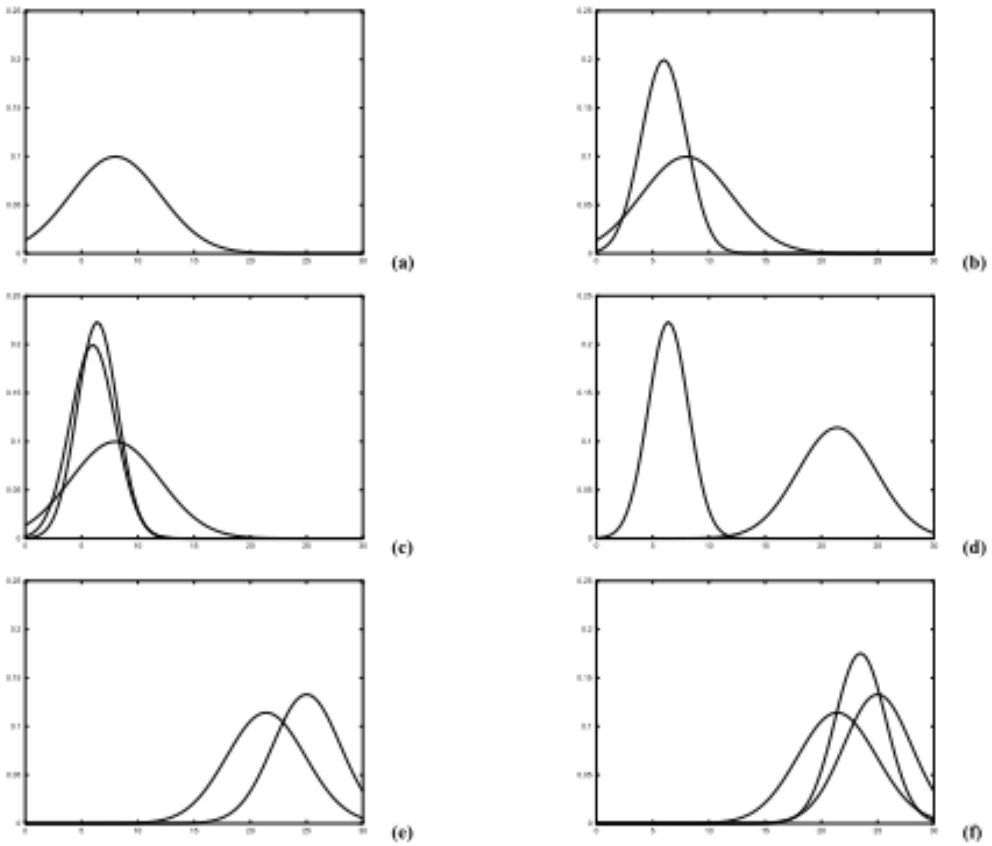

Figure 2.5: Illustration of the Kalman Algorithm in a single axis movement[13].

The main disadvantages of the KF are the assumptions of linear state transitions and measurements with additive Gaussian noise, conditions that are rarely satisfied in practice. The assumption of linearity is overcome by the Extended Kalman Filter (EKF), which inherits the basic belief representation of the KF, with the difference being that the belief is linearized via Taylor expansion.

Since the EKF is computationally efficient[13], it is commonly used for state estimation in robotics, and UUV localization is no exception. The EKF is widely used with many localization techniques [2], as well as in many single beacon localization implementations [14], [4] and in CN [10].

The Particle Filter (PF) is a nonparametric implementation of the Bayes Filter [13]. The key idea behind the PF is representing a probability distribution by a set of random samples drawn from it. This representation is not parametric, so it can represent any distribution of probability. However, it is important to refer that these distributions are always approximations.

In a Particle Filter, state belief is represented by a set of sample states known as particles, commonly denoted as $x_t^{[m]}$, where m is the index of the particle. Each of these particles are a hypothesis of the real state at a time t. Each set of particles $\mathscr{X}_{t+1}$ is constructed using the previous set $\mathscr{X}_{\sqcup}$.

When a measurement z_t is taken, a weight $w_t^{[m]}$ is associated to each particle. The weight $w_t^{[m]}$ of a particle is given by the conditional probability of z_t given $x_t^{[m]}$. After incorporating the measurement into the current distribution of particles, these are resampled, taking into account the weights of each particle.

The main disadvantages of the particle filter are the approximation errors related to the fact that a finite number of particles must be used and the errors introduced by the randomness in resampling. A large number of particles decreases these disadvantages, but significantly increases the computational cost, since the algorithm's complexity is $\mathscr{O}(M^N)$ [13].

The particle filter has been used successfully in different approaches to UUV acoustic localization [15] [16], including single beacon techniques [17].

As mentioned above, both the EKF and PF have been used in single beacon UUV localization. The main shortcoming of the EKF is the assumption of Gaussian noise, while the limitations of the PF originate from the particle number limit imposed by the computational resources available, due to the algorithm's complexity.

Since the particle filter's performance is so heavily influenced by the computational power of the device that will run it, it is not possible to determine *a priori* the filter with best performance. It is common to see comparisons between these filters in many underwater localization problems , such as [11], [18] or [4]. In other cases, the solution proposed is a combination of both [16].

2.3.2 Cramer-Rao Lower Bound

.

The Cramer-Rao Lower Bound (CRLB) is a tool used for determining the minimum uncertainty achievable by an optimal estimator based on the uncertainty of measurements and a model

relating the measurements to the parameters to estimate. The CRLB is commonly used in this area since localization is an estimation problem, where the position and attitude of a vehicle are estimated based on certain measurements. [1].

While the CRLB can be used as a metric for the performance of an implemented estimator, as mentioned in [1], it is common to use it in observability studies [19] and as a parameter for design purposes [20]. The Fisher Information Martix (FIM) is used as a sensor placement metric in [21].

Chapter 3

System concept

The main purpose of this dissertation, as mentioned in chapter 1, is the development of guidance algorithms for an Autonomous Surface Vehicle (ASV) to improve the position estimate of a ROV in a cooperative navigation system. It is established that when using only one acoustic beacon the observability of the UUV's parameters depends on the relative positions of the UUV and ASV. Operating the ROV for long periods of time without constraints regarding its path is one of the main reasons to use a single moving beacon, hence the importance of the guidance algorithm.

3.1 Vehicle Overview

The guidance algorithm in this dissertation is not intended to be implemented in any particular vehicle. However, certain assumptions about the vehicles are made in order to narrow down possible scenarios.

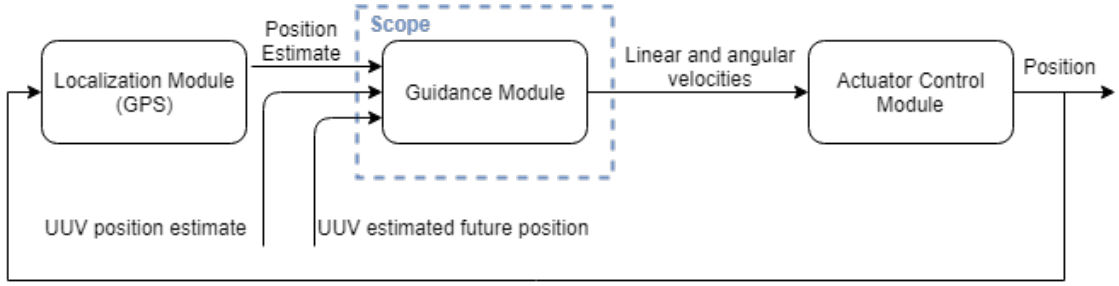

Figure 3.1: Model for the surface vehicle.

Regarding the ASV, the existence of a localization module is assumed, giving it the ability to determine its position with a certain uncertainty. It is also assumed that a control module for the vehicle's actuators is also implemented, meaning that the only input needed to move the ASV are the desired linear and angular velocities. As a result, the scope of this work regarding the ASV, as highlighted in figure 3.1, is solely the development of a guidance algorithm that determines the position where the acoustic ranges contribute to minimize the uncertainty of the UUV's position

estimate. The inputs for this algorithm are the current position estimate of the ASV, the current position estimate of the UUV and estimates of the future UUV position.

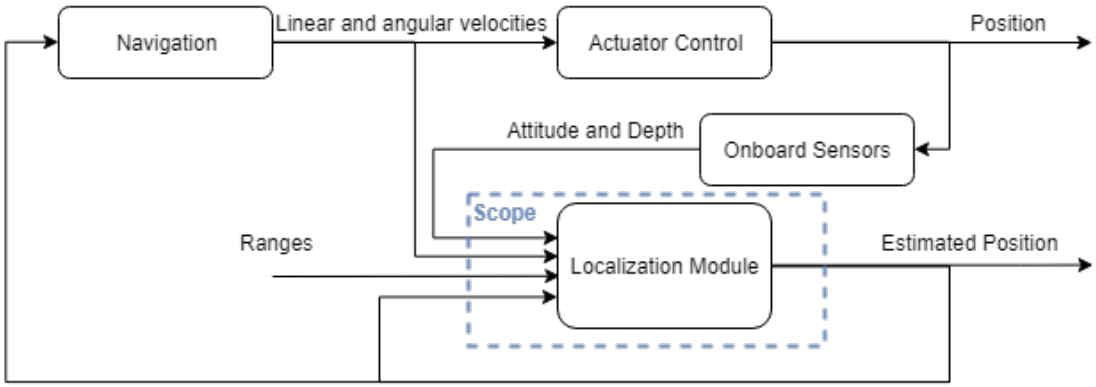

Figure 3.2: Model for the underwater vehicle.

The first assumption made about the underwater vehicle is that it is remotely operated. The scope of this work regarding the ROV is the development of a localization module, as shown in figure 3.2. A control module is assumed to be implemented as was the case with the ASV. Since the vehicle is remotely operated, the navigation is carried out by a human. The inputs for the localization module are the current ROV position estimate, the current UUV speed estimate, current position information (from on board sensors, such as a gyroscope and/or compass) and ranges to the ASV.

Using a ROV means that there is communication between the vehicles, which in turn implies two key assumptions. First of all, the range can be determined using OWTT, since the vehicles are synchronized. Secondly, it can be assumed that both vehicles have access to each others' position estimate. This is a key factor for two reasons:

- To use the ranges to the surface vehicle to improve its position estimate, the ROV must have information about the position of the surface vehicle.
- One of the inputs of the ASV's guidance algorithm is the current and future position of the ROV

While it would be possible to develop a solution for a scenario where no communication between the vehicles is established, the uncertainty of the localization would likely increase, since each vehicle would have to maintain an estimate of the other vehicle's position.

3.2 Underwater Vehicle Localization

In order to estimate the position of the ROV an Extended Kalman Filter was used. As can be seen in 3.2, in order to predict the vehicle's next position the following information was used:

- the vehicles current position estimate;

- estimate of the vehicle's angular and linear speed;
- measurements of the vehicle's attitude and depth given by onboard sensors;
- ranges to the ASV (when available);

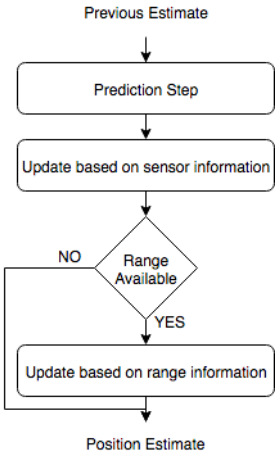

Figure 3.3: Algorithm of the implemented Extended Kalman Filter.

The algorithm of the EKF is shown in figure 3.3. The equations for the EKF are exposed in [13]. Since the measurements of the attitude and depth of the vehicle have low uncertainty they are used to update the prediction calculated using the vehicle's velocity estimate. Whenever a new range is available, the state prediction is corrected based on it. The transition model used in the prediction step is the one in (3.1), where Δt is the duration of a simulation step.

$$X(k+1) = \begin{bmatrix} N(k+1) \\ E(k+1) \\ D(k+1) \\ \phi(k+1) \\ \theta(k+1) \\ \psi(k+1) \end{bmatrix} = f(X(k),u(k)) + \mathcal{N}(0,Q(k)) \tag{3.1}$$

$$f(X(k),u(k)) = \Delta t \cdot J(X(k))u(k)$$

The detailed expressions for $f(X(k),u(k))$, $\nabla f_x(\hat{X}(k),u(k))$ and $\nabla f_u(\hat{X}(k),u(k))$ are shown in appendix A. Based on this transition model the next state can be predicted using the equations shown in (3.2) to compute the expected value and covariance of the pose prediction.

$$\begin{aligned} \hat{X}(k+1|k) &= \hat{X}(k) + \Delta t \cdot J(\hat{X}(k))\hat{u}(k)) \\ P(k+1|k) &= \nabla f_X(\hat{X}(k),u(k)) \cdot P(k) \cdot \nabla f_X^T(\hat{X}(k),u(k)) + \nabla f_u(\hat{X}(k),u(k)) \cdot Q \cdot \nabla f_u^T(\hat{X}(k),u(k)) \end{aligned} \tag{3.2}$$

The next step is the inclusion of measurements given by the on board sensors, which include measurements of the attitude and depth of the vehicle. These measurements can be written in function of the state, as shown in equation (3.3)

$$\begin{gathered} M(k) = \begin{bmatrix} D \\ \phi \\ \theta \\ \psi \end{bmatrix} = h_m(X(k)) + \mathcal{N}(0, R_s) \\ h_m = \begin{bmatrix} D \\ \phi \\ \theta \\ \psi \end{bmatrix} \end{gathered} \tag{3.3}$$

The expected measurement considering the state estimate and its covariance can be expressed as

$$\begin{gathered} \hat{M}(k) = h_m(\hat{X}(k)) \\ S_1(k) = \nabla h_m(\hat{X}(k)) \cdot P(k) \cdot \nabla h_m(\hat{X}(k))^T + R \end{gathered} \tag{3.4}$$

$$K_1(k) = P(k+1|k) \cdot \nabla h_m(\hat{X}(k))^T \cdot S_1(k)^{-1} \tag{3.5}$$

With these values the kalman gain for this update can be calculated through equation (3.5), in order to update the state prediction, using the equations in (3.6).

$$\begin{gathered} \hat{X}(k+1|k+1) = \hat{X}(k+1|k) + K_1(k) \cdot (M(k) - \hat{M}(k)) \\ P(k+1|k+1) = [I - K_1(k) \nabla h_m(\hat{X}(k+1))] \cdot P(k+1|k) \end{gathered} \tag{3.6}$$

Whenever a range measurement is available it must also be incorporated into the state prediction. To accomplish this a second update is made. The range can be expressed in function of the state variables using (3.7). Using this knowledge the expected measurement $\hat{Z}(k)$ and respective covariance can be calculated using (3.8).

$$\begin{gathered} Z(k) = h_z(X(k)) + \mathcal{N}(0, R_r) \\ h_z = \sqrt{(N_{ROV} - N_{ASV})^2 + (E_{ROV} - E_{ASV})^2 + D_{ROV}^2} \end{gathered} \tag{3.7}$$

$$\begin{gathered} \hat{Z}(k) = h_z(\hat{X}(k)) \\ S_2(k) = \nabla h_z(\hat{X}(k)) \cdot P(k) \cdot \nabla h_z(\hat{X}(k))^T + R \end{gathered} \tag{3.8}$$

The final steps to obtain the updated state prediction are the calculation of the Kalman gain and of the expected value and covariance for the next state.

$$K_2(k) = P(K) \cdot \nabla h_z(\hat{X}(k))^T \cdot S_2(k)^{-1} \tag{3.9}$$

State and covariance update

$$\begin{aligned} \hat{X}(k+1|k+1) &= \hat{X}(k+1|k+1) + K_2(k) \cdot (Z(k) - \hat{Z}(k)) \\ P(k+1|k+1) &= [I - K_2(k)\nabla h_z(\hat{X}(k))] \cdot P(k+1|k+1) \end{aligned} \tag{3.10}$$

3.3 Surface Vehicle Guidance

The guidance of the surface vehicle is done by establishing waypoints for instants in time when acoustic signals are sent. Since the trajectory of the vehicle is decided in real time during the missions, the computation of the waypoints is an iterative process, meaning that whenever a signal is sent, the next waypoint is determined.

The first step to determine the next waypoint is the definition of the surface vehicle's reaching set. A reaching set is the set of points on the sea surface the vehicle can reach in a given time. The reaching set of an omnidirectional vehicle is shown in figure 3.4. The value of R depends on the maximum velocity of the vehicle and travelling time.

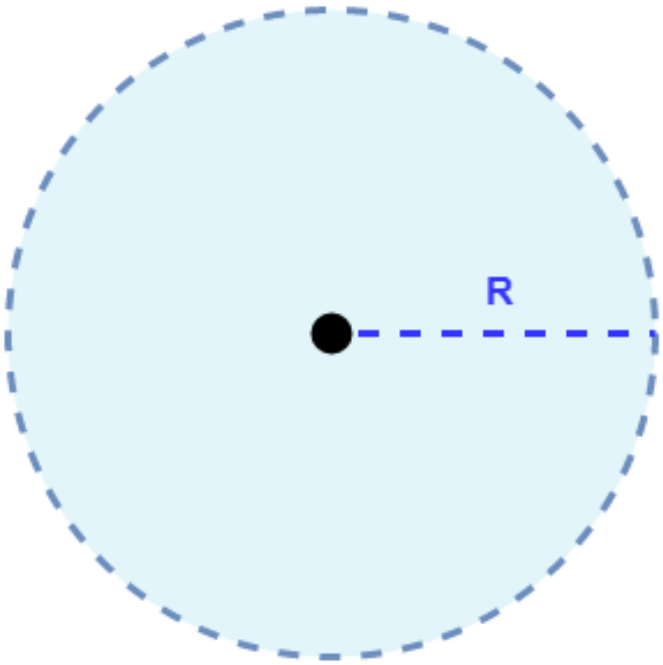

Figure 3.4: Surface vehicle reaching set

In short, after the surface vehicle send an acoustic signal, its reaching set is calculated using amount of time until the next range and the maximum velocity of the vehicle. It is assumed that the surface vehicle is holonomic, even though that is not the case in many real scenarios. After that, the target point is chosen from the reaching set, according to the metrics based on the analysis of the FIM, which will be described ahead,

3.3.1 Information of range measurements

The first step to create a guidance algorithm is to find a tool to quantify the influence of the relative position of the ASV and ROV in the parameters to estimate. To that end, the range measurement can be written in function of the positions of the ROV and ASV, as shown in (3.11). From this point, the subscripts 'ASV' and 'ROV' are used in variables to refer to the surface and underwater vehicle, respectively.

$$Z = \sqrt{(N_{ROV} - N_{ASV})^2 + (E_{ROV} - E_{ASV})^2 + D_{ROV}^2} \tag{3.11}$$

Considering $w = (N_{ROV}, E_{ROV})$ as the parameters to estimate, the amount of information that the measurement carries about w can be quantified using the Fisher information matrix. Assuming Gaussian and independent measurement errors, the information matrix is given by (3.12). [20]

$$\imath(w) = \nabla_w Z(w)^T Q^{-1} \nabla_w Z(w) \tag{3.12}$$

The Jacobian of the measurement with respect to the parameters to be estimated is shown in equation (3.13).

$$\nabla_w Z_w = \begin{bmatrix} \frac{N_{ROV} - N_{ASV}}{Z} & \frac{E_{ROV} - E_{ASV}}{Z} \end{bmatrix} \tag{3.13}$$

The assumption that the ROV is stationary between consecutive range measurements to the ASV in different positions creates a synthetic baseline scenario. The information carried by these measurements about the parameters to be estimated is given by the summation of the information matrices of each measurement, as shown in (3.14). For this equation to be valid, the variance of the measurement errors has to be considered equal for both ranges.

$$\imath(w) = \frac{1}{\delta^2} \sum_{i=1}^{N} \begin{bmatrix} \frac{(N_{ROV} - N_{ASVi})^2}{Z_i^2} & \frac{(N_{ROV} - N_{ASVi})(E_{ROV} - E_{ASVi})}{Z_i^2} \\ \frac{(N_{ROV} - N_{ASVi})(E_{ROV} - E_{ASVi})}{Z_i^2} & \frac{(E_{ROV} - E_{ASVi})^2}{Z_i^2} \end{bmatrix} \tag{3.14}$$

Using the FIM, the minimum uncertainty of the estimate $\hat{w}$ of the parameter w based on this measurement can be determined, since the Cramer-Rao Lower Bound ($\mathscr{C}$) is equal to the inverse of the FIM ($\imath$). $\mathscr{C}$ defines an uncertainty ellipsoid, the volume of which is a measurement of the uncertainty of $\hat{w}$. The determinant of the information matrix is used as a measure of the volume of the uncertainty ellipse, meaning that maximizing the determinant $det(\imath(w))$ minimizes the uncertainty of $\hat{w}$. [20].

With this premises, two metrics were constructed to use in the choice of the waypoints.

3.3.2 Approach A

The determinant of the information matrix (3.14) considering one position of the ROV and N positions of the ASV is given by equation (3.15).

$$det(\imath(w)) = \frac{1}{\delta^2}\sum_{i=1}^{N}\frac{(N_{ROV}-N_{ASVi})^2}{Z_i^2} * \sum_{i=1}^{N}\frac{(E_{ROV}-E_{ASVi})^2}{Z_i^2} - (\sum_{i=1}^{N}\frac{(N_{ROV}-N_{ASVi})(E_{ROV}-E_{ASVi})}{Z_i^2})^2 \quad (3.15)$$

In this approach, only the current position of the ASV is used to determine the next waypoint, meaning that $N = 2$. This implicates that the next position of the ASV is determined using only the current positions of the ASV and ROV. The determinant of the information matrix is then considered as a function of the next position of the surface vehicle, which makes it possible to discover the position where $det(\imath(w))$ is maximized and, consequently, the uncertainty of $\hat{w}$ is minimized. A surface plot of the determinant in function of the ASV's next waypoint is shown in figure 3.5. In this case, the ROV is considered to be in position (0, 0, -20) and the ASV's coordinates are (20, 20).

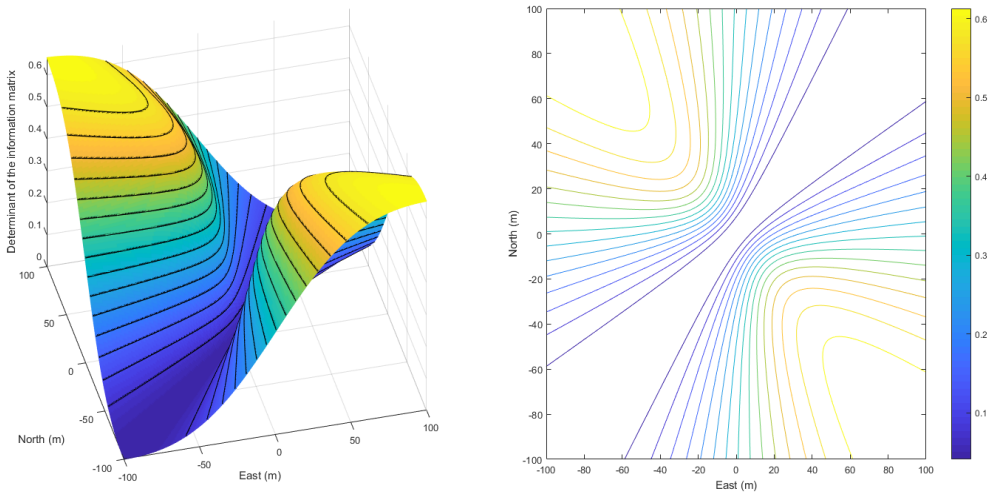

Figure 3.5: Determinant of the information matrix in function of the ASV's next position.

An example of the behaviour of the guidance algorithm using this metric is shown in figure 3.6. As previously explained, whenever the surface vehicle (black cross) reaches a waypoint and sends an acoustic signal, the determinant of the information matrix is calculated for all the points within the surface vehicle's reaching set (every point inside the black circumference). The next waypoint is the point among these that maximizes the determinant of the FIM.

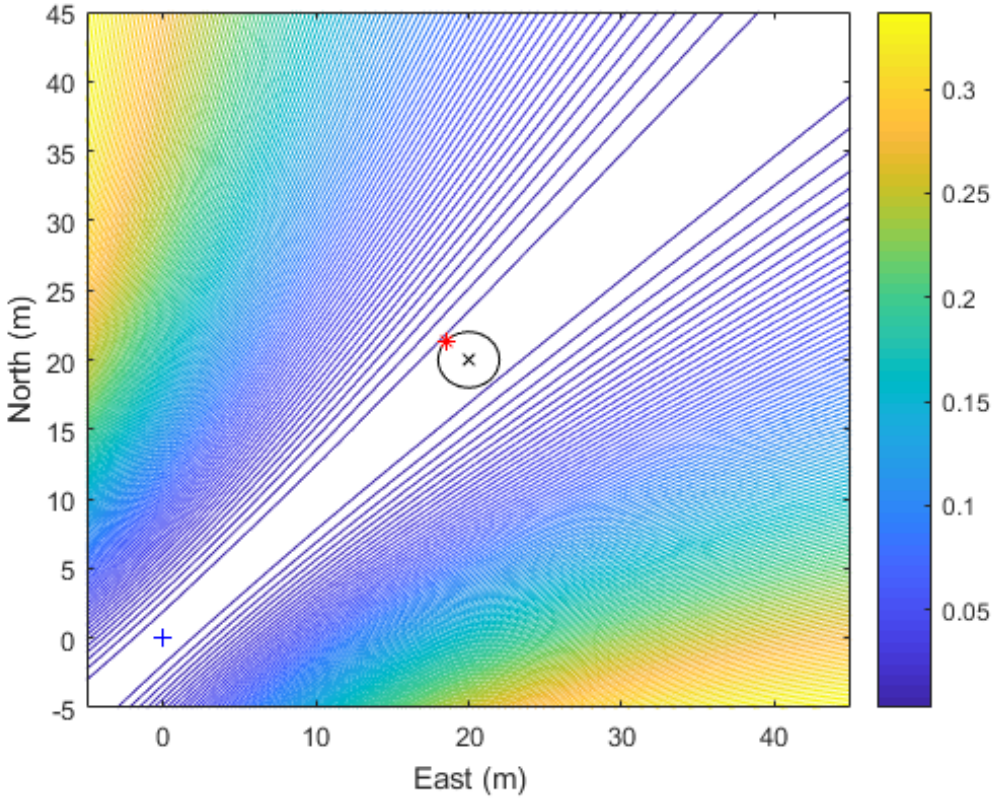

Figure 3.6: Graphic example of the SV next position.

3.3.3 Approach B

This approach was developed since the assumption that the ROV is stationary is not always true. In the previous approach, only the current positions of the ROV (X_{ROV1}) and ASV (X_{ASV1}) are used to determine the next waypoint of the ASV (X_{ASV2}). However, the fact that the ROV may move to another position (X_{ROV2}) is considered in that metric.

Since the relative positioning of the ROV and ASV when ranges are sent is a key factor in the uncertainty of $\hat{w}$, the inclusion of an estimate of X_{ROV2} in this metric may have a positive effect in lowering said uncertainty. This effect is naturally limited by the accuracy of the X_{ROV2} estimate.

In order to take into account the change of the position of the ROV, both positions are considered as separate parameters to estimate. These are refereed to as $w1 = (N_{ROV1}, E_{ROV1})$ and $w2 = (N_{ROV2}, E_{ROV2})$. To address this situation, two FIMs are defined, shown in (3.16) and (3.17).

$$\iota(w1) = \frac{1}{\delta^2}\sum_{i}^{2}\begin{bmatrix} \frac{(N_{ROV1}-N_{ASVi})^2}{Z_i^2} & \frac{(N_{ROV1}-N_{ASVi})(E_{ROV1}-E_{ASVi})}{Z_i^2} \\ \frac{(N_{ROV1}-N_{ASVi})(E_{ROV1}-E_{ASVi})}{Z_i^2} & \frac{(E_{ROV1}-E_{ASVi})^2}{Z_i^2} \end{bmatrix} \tag{3.16}$$

$$\iota(w2) = \frac{1}{\delta^2}\sum_{i}^{2}\begin{bmatrix} \frac{(N_{ROV2}-N_{ASVi})^2}{Z_i^2} & \frac{(N_{ROV2}-N_{ASVi})(E_{ROV2}-E_{ASVi})}{Z_i^2} \\ \frac{(N_{ROV2}-N_{ASVi})(E_{ROV2}-E_{ASVi})}{Z_i^2} & \frac{(E_{ROV2}-E_{ASVi})^2}{Z_i^2} \end{bmatrix} \tag{3.17}$$

As was the case in the previous approach, the determinant of both matrices are a measurement of the uncertainty of the estimates. The determinants of both matrices are shown in (3.18).

$$
\begin{aligned}
det(\iota(w1)) &= \frac{1}{\delta^2}\sum_i^2 \frac{(N_{ROV1}-N_{ASVi})^2}{Z_i^2} * \sum_i^2 \frac{(E_{ROV1}-E_{ASVi})^2}{Z_i^2} - (\sum_i^2 \frac{(N_{ROV1}-N_{ASVi})(E_{ROV1}-E_{ASVi})}{Z_i^2})^2 \\
det(\iota(w2)) &= \frac{1}{\delta^2}\sum_i^2 \frac{(N_{ROV2}-N_{ASVi})^2}{Z_i^2} * \sum_i^2 \frac{(E_{ROV2}-E_{ASVi})^2}{Z_i^2} - (\sum_i^2 \frac{(N_{ROV2}-N_{ASVi})(E_{ROV2}-E_{ASVi})}{Z_i^2})^2
\end{aligned}
\tag{3.18}
$$

Since the global objective of this work is to minimize the uncertainty of position of the ROV at all times, the metric defined in this approach is the sum of the determinants, show in (3.19).

$$
m = det(\iota(w1)) + det(\iota(w2)) \tag{3.19}
$$

For a better understanding of how m varies according to the next waypoint of the ASV, in figure 3.7 this metric is shown in function of the surface vehicle's next position, considering that the ROV moves from position [0, 0 -20] to [20, 0, -20] and that the current position of the ASV is [20, 0].

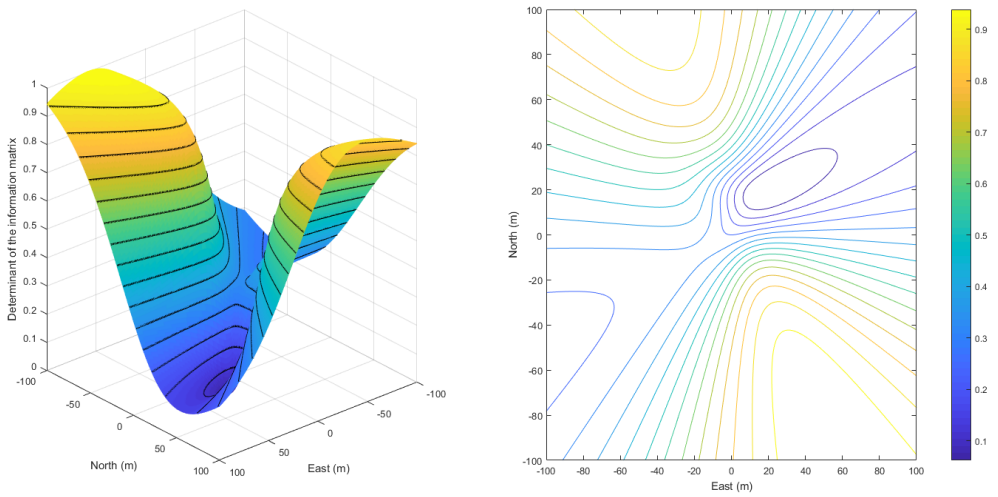

Figure 3.7: Sum of the determinants in function of the ASV's next position.

An example of the behaviour of the guidance algorithm using this metric is shown in figure 3.8. Whenever the surface vehicle (black cross) reaches a waypoint and sends an acoustic signal, the metric is calculated for all the points within the surface vehicle's reaching set (every point inside the black circumference). The next waypoint is the point among these that maximizes the metric.

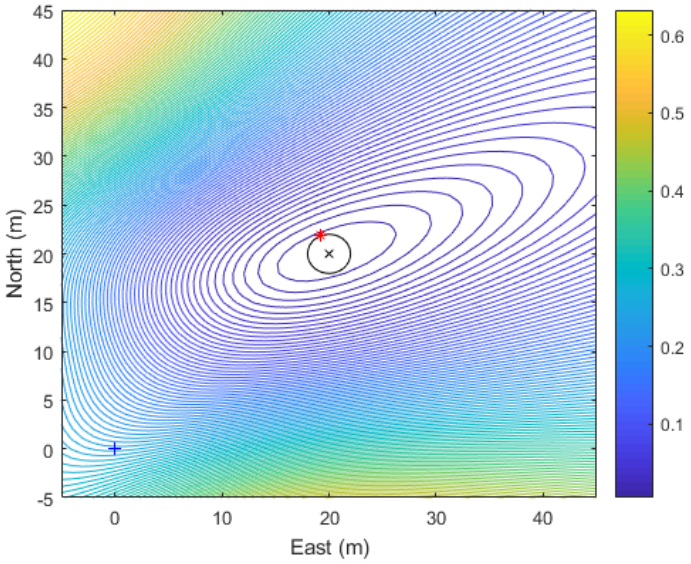

Figure 3.8: Graphic example of the SV next position.

Chapter 4

Simulation and Results

4.1 Simulation Environment

To test the guidance algorithm and metrics exposed in 3, a simulation environment was created. In this section, the algorithm shown in figure 4.1 is explained in detail to give a comprehensive view of the construction of this simulation environment.

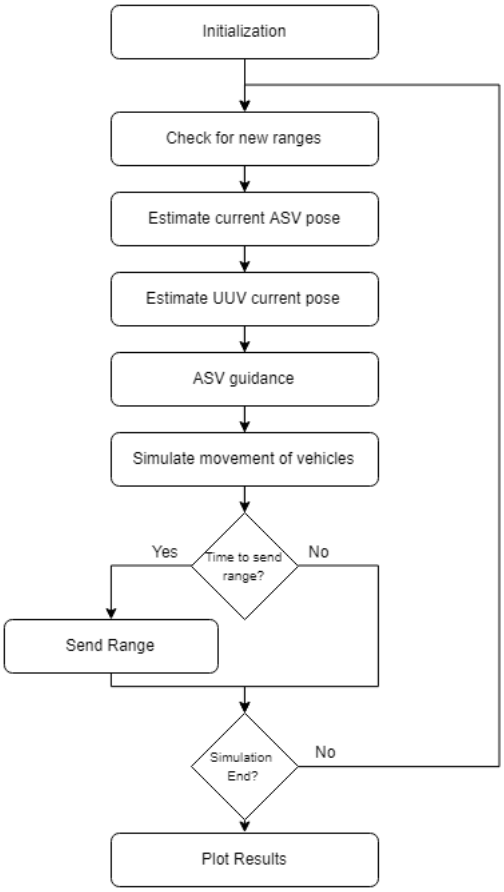

Figure 4.1: Flowchart of the simulation algorithm.

In the initialization phase simulation parameters such as the simulation time, simulation step, time between acoustic ranges and initial positions of the vehicles are defined. The inputs for the ROV (the linear and angular velocities) are also defined in this step. The next steps in the algorithm, including the models used to simulate the vehicles as well as localization and guidance algorithms are explained in detail throughout the chapter.

4.1.1 Vehicle Simulation

The motion of the vehicles is modelled as shown in chapter 2. In order to simulate the motion of the vehicles, kinematic equations were used [12]. To simulate the behaviour of an autonomous surface vehicle the kinematic model shown in equation (4.1) was used. As previously mentioned, position and attitude of the vehicle are expressed through vector $X_{ASV} = [N_{ASV}, E_{ASV}, \psi_{ASV}]^T$. The linear and angular velocities are expressed in vector $\nu_{ASV} = [u_{ASV}, v_{ASV}, r_{ASV}]^T$.

$$\dot{X}_{ASV} = J_{ASV}(X_{ASV})u_{ASV} \tag{4.1}$$

The transformation matrix for the surface vehicle J_{ASV} is the transformation matrix between the body-fixed and NED reference frames and shown in equation (4.2) [12].

$$J_{ASV} = \begin{bmatrix} cos(\psi_{ASV}) & -sin(\psi_{ASV}) & 0 \\ sin(\psi_{ASV}) & cos(\psi_{ASV}) & 0 \\ 0 & 0 & 1 \end{bmatrix} \tag{4.2}$$

To simulate the motion of the Surface Vehicle the differential equation (4.1) was solved in each simulation step using ode45, a function available in MatLab which implements the Dorman-Prince method.

In addition to simulating the motion of the surface vehicle, the localization method of the surface vehicle has to be simulated as well. Since it was assumed that a localization system was already implemented, the position estimate of the ASV ($\hat{X}_{ASV}$) is determined by adding a random value within the expected error of the localization system to the true position of the vehicle (X_{ASV}), as shown in (4.3).

$$\hat{X}_{ASV}(k) = X_{ASV}(k) + \varepsilon_{GPS} \tag{4.3}$$

The motion of the ROV was simulated using the kinematic model shown in (4.4). As was explained in chapter 2, the position and attitude of the vehicle are expressed through vector $X_{ROV} = [N_{ROV}, E_{ROV}, D_{ROV}, \theta_{ROV}, \phi_{ROV}, \psi_{ROV}]^T$ and its linear and angular velocities are expressed in vector $\nu_{ROV} = [u_{ROV}, v_{ROV}, w_{ROV}, p_{ROV}, q_{ROV}, r_{ROV}]^T$.

$$\dot{X}_{ROV} = J_{ROV}(X_{ROV})u_{ROV} \tag{4.4}$$

The transformation matrix for the underwater vehicle J_{ROV} is the transformation matrix between the body-fixed and NED referentials [12] and is shown in (4.5).

The simulation of the ROV's motion was similar to the simulation of the surface vehicle,i.e. the differential equation (4.4) was solved in each simulation step using the Dorman-Prince method, implemented in MatLab's function ode45. Using this method of simulating the vehicle means that its path is defined by the inputs provided in the initialization (linear and angular velocities throughout the simulation).

$$\begin{bmatrix} c(\psi)c(\theta) & c(\psi)s(\theta)s(\phi)-s(\psi)c(\phi) & s(\psi)s(\phi)+c(\psi)c(\phi)s(\theta) & 0 & 0 & 0 \\ s(\psi)c(\theta) & c(\psi)c(\phi)+s(\phi)s(\theta)s(\psi) & s(\theta)s(\psi)c(\phi)-c(\psi)s(\phi) & 0 & 0 & 0 \\ -s(\theta) & c(\theta)s(\phi) & -(\theta)c(\phi) & 0 & 0 & 0 \\ 0 & 0 & 0 & 1 & s(\phi)t(\theta) & c(\phi)t(\theta) \\ 0 & 0 & 0 & 0 & c(\phi) & -s(\phi) \\ 0 & 0 & 0 & 0 & \frac{s(\phi)}{c(\theta)} & \frac{c(\phi)}{c(\theta)} \end{bmatrix} \tag{4.5}$$

The estimation of the ROV's state ($\hat{X}_{ROV}$) was obtained by implementing an Extended Kalman Filter, as described in chapter 3. The simulation of the sensor readings and acoustic ranges is obtained by adding a random value within the expected error of the sensor to the true value of the variable. The true value of the variables measured by on board sensors (attitude and depth) is taken directly from the state vector (X_{ROV}). The method for obtaining the true value of the ranges is explained in 4.1.2.

4.1.2 Range

There is particular focus on the simulation of the acoustic ranges because during the time elapsed since a signal is sent by the ASV until it is received by the ROV both vehicles may move, therefore obtaining the range is not simply calculating the distance between the vehicles at a given point in time.

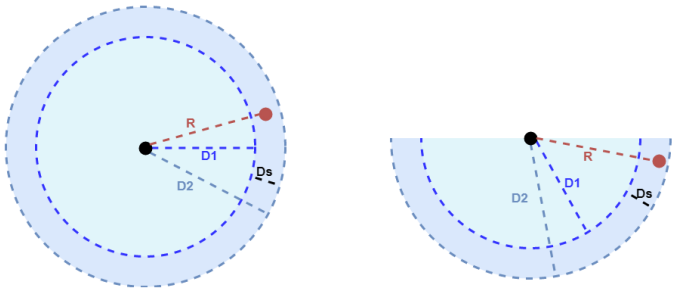

Figure 4.2: Top and lateral views of an example position of the ROV relative to the signal origin

To deal with this problem, information about each range is stored in a data structure with $[X_{ASV}, state, r]$, where X_{ASV} is the position of the surface vehicle at the time the signal was sent, the variable state keeps track of whether the signal has been received and r is the distance traveled by the signal (or the value of the range if the signal has already been received).

In figure 4.2 an example position of the ROV (represented as the red dot) relative to the origin of the signal (black dot) is shown in two perspectives (top view on the left side of the image and side view on the right side).

At each simulation step the distance that a signal could have traveled during the step is calculated (Ds), which is added to the distance already travelled by that signal ($D1$), to calculate the total distance travelled by the signal ($D2$). Using this value, the position of the ASV when the signal was sent and the current position of the ROV, it is determined whether or not the ROV has received the signal. If the signal has been received, the variable state is updated and the distance between the point where the ASV sent the signal and the current position of the ROV (R) is computed and stored.

Calculating the range R is necessary because otherwise the precision of the ranges would be limited by Ds, which is proportional to the simulation step time. Calculating the range value directly allows for precise ranges without the need for low simulation step time, decreasing the computational effort.

4.2 Simulation Results

The guidance algorithms were tested in the simulation environment with the ROV stopped and moving in three different paths, shown in figure 4.3. In all of the tests a two hour mission was simulated.

Both guidance algorithms were tested using these paths, with different starting points of the ROV and ASV. The results of the simulations are analyzed in light of the mean and variance of the position estimation error. Since the parameters to estimate are the coordinates of the ROV in the horizontal plane (NE), the estimation error is given by (4.6)

$$\varepsilon = \sqrt{(X_{ROV} - \hat{X}_{ROV})^2 + (Y_{ROV} - \hat{Y}_{ROV})^2} \tag{4.6}$$

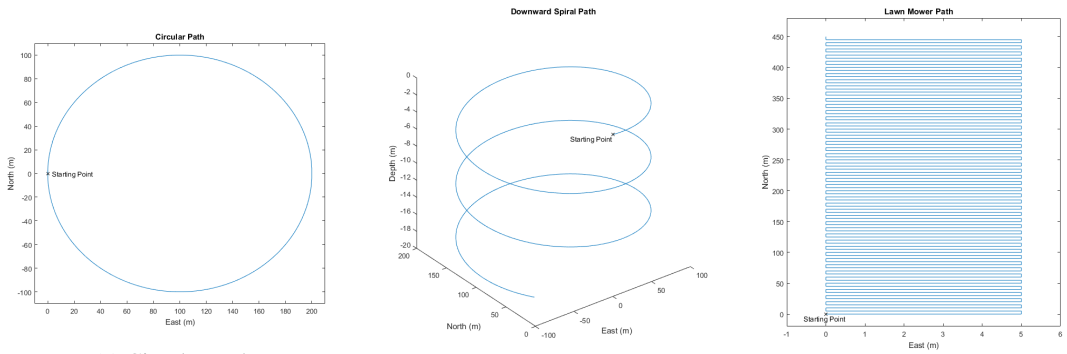

(a) Circular Path

(b) Downward Spiral Path

(c) Lawn mower path

Figure 4.3: Different paths of the ROV used to test the guidance algorithms.

4.2.1 Approach A

The first tests presented are two tests where the starting position of the ROV is the same (0, 0, -5) but the path followed is different. It can be clearly seen that when the ROV follows a circular path (4.4a) the error is bounded, while in the case the path performed is a spiral (4.4b), the positioning error increases.

Since the main difference between these paths is the increasing depth in the spiral path, the increasing error implicates that the depth of the ROV may have an effect on the positioning error.

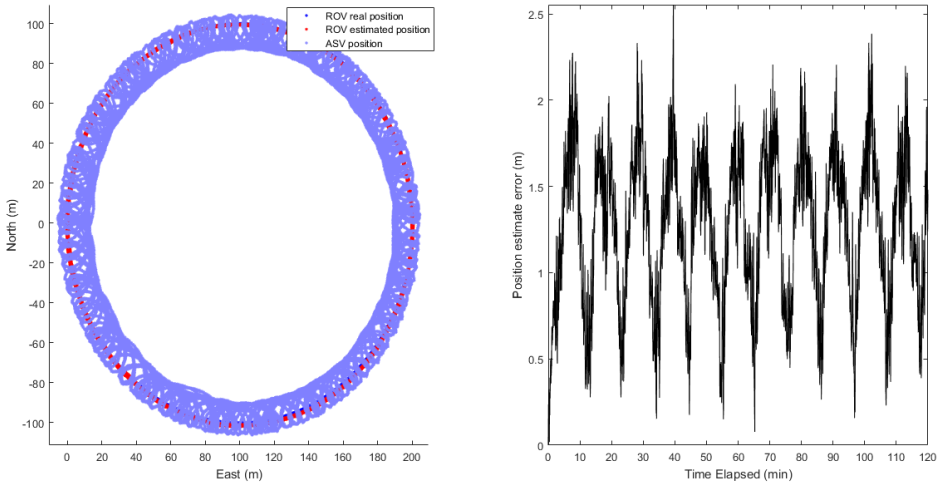

(a) Test with circular path

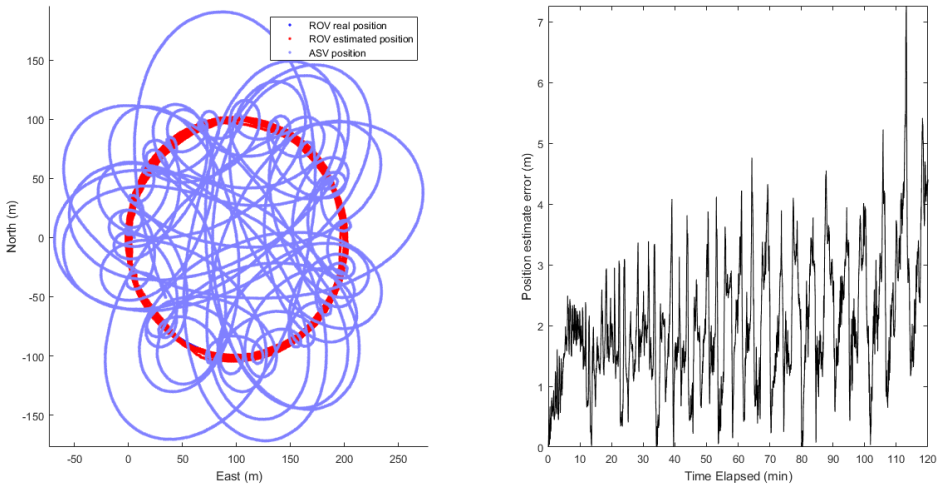

(b) Test with the spiral path

Figure 4.4: Comparison between two tests with the ROV following the circular and spiral paths.

The tests shown in figure 4.5, where the starting point of the ASV is (0,20) and ROV is stationary in two different points: (0, 0, -5) and (0, 0 , -20).

On the one hand, the fact that the error is greater in 4.5b supports the previous statement that the depth of the ROV has an effect on the estimation error.

On the other hand, it is noticeable that the horizontal distance the ASV keeps from the ROV is also different in both scenarios. The term horizontal distance is used to refer to the distance between the ASV and ROV in the NE plane, calculated using (4.7)

$$\sqrt{(N_{ROV} - N_{ASV})^2 + (E_{ROV} - E_{ASV})^2} \tag{4.7}$$

The fact that in figure 4.5a the ASV approaches the ROV until a certain distance and in figure 4.5b it keeps the original distance indicates that the horizontal distance between the ROV and ASV may also be a factor that influences the error of the estimate.

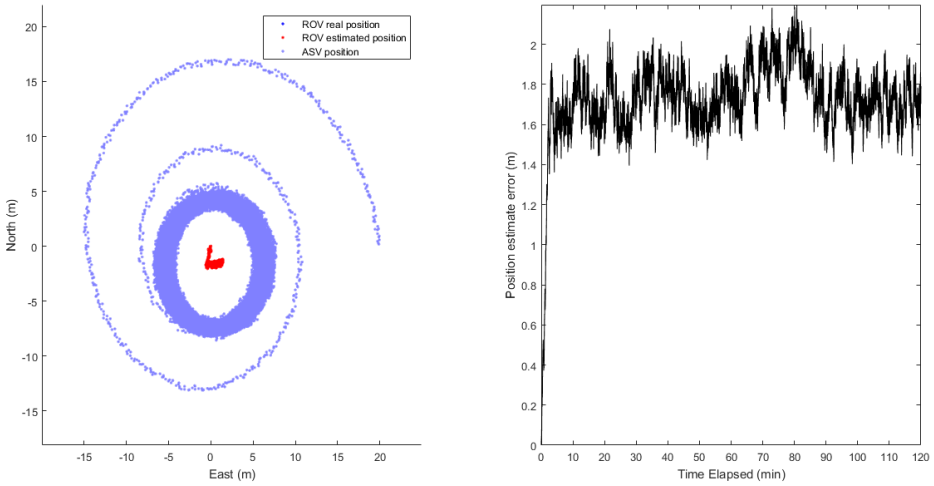

(a) Test with the ROV stationary in (0,0,-5)

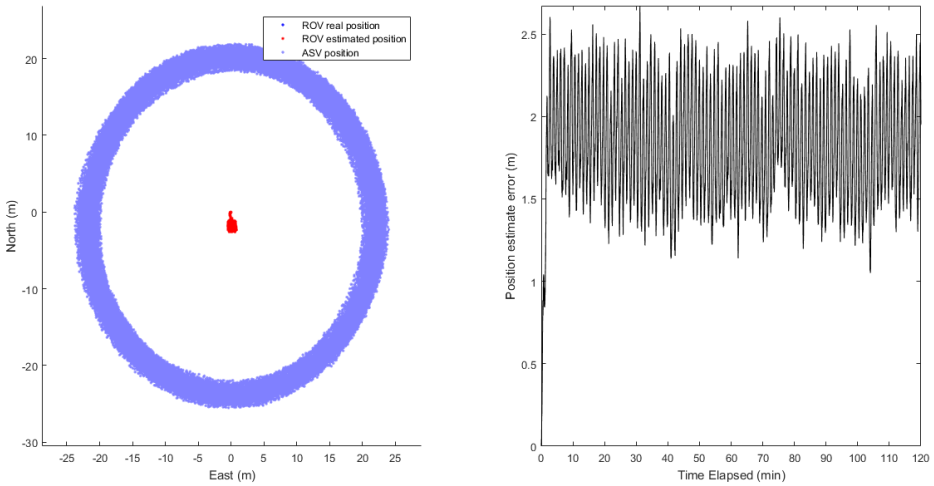

(b) Test with the ROV stationary in (0,0,-20)

Figure 4.5: Comparison between two tests with the ROV stationary at different depths.

To infer about the validity of the previous assessments about the influence of the depth of the ROV in the estimation error, an analysis of the metric defined in 3.3.2 is made.

As mentioned in 3.3.1, the determinant of the information matrix is a measurement of the uncertainty of the estimation of the horizontal position of the ROV (N and E coordinates) based on two range measurements. In figure 4.6, four surface plots of the determinant in function of the position of the ASV in the second range are shown. The differences between them are the positions of the ROV and ASV in the first range.

Upon interpreting these plots, it becomes apparent that the determinant of the information matrix is maximum when the depth of the ROV is low and the horizontal distance between the ASV and ROV is high. However, the global maximum determinant of the information matrix is not an indicator of the uncertainty in the obtained estimation. The direct measurement of the minimum uncertainty of the estimate is the maximum determinant within the reaching set of the ASV.

For example, while the maximum value of the determinant of the FIM in figure 4.6b is higher than the maximum in figure 4.6a, there is no guarantee that the maximum determinant of the FIM within the reaching set of the ASV is also higher.

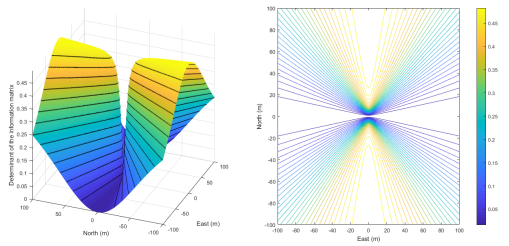

(a) ROV (0, 0, -5); ASV (0, 5)

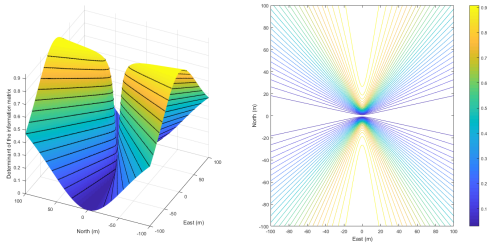

(b) ROV (0, 0, -5); ASV (0, 20)

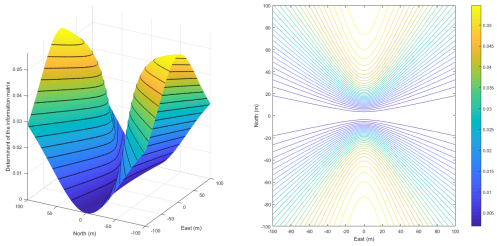

(c) ROV (0, 0, -20); ASV (0, 5)

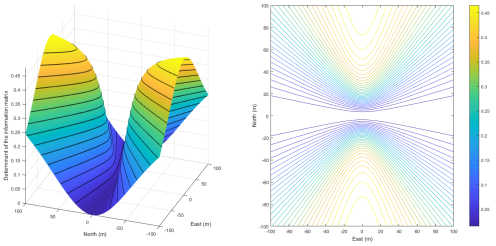

(d) ROV (0, 0, -20); ASV (0, 20)

Figure 4.6: Determinant of the FIM in function of the next position of the ASV for different depths and ASV positions.

After these tests it is possible to conclude that there is a relation between the uncertainty of the estimate in the first pair of ranges, the depth of the ROV, the distance between the ROV and ASV and the speed of the ASV.

Given the existence of this relation, for any given depth of the ROV it is possible to determine a horizontal distance between the vehicles that minimizes the uncertainty for the first two ranges, as long as the reaching set of the ASV is well defined, that is, as long as the time between the

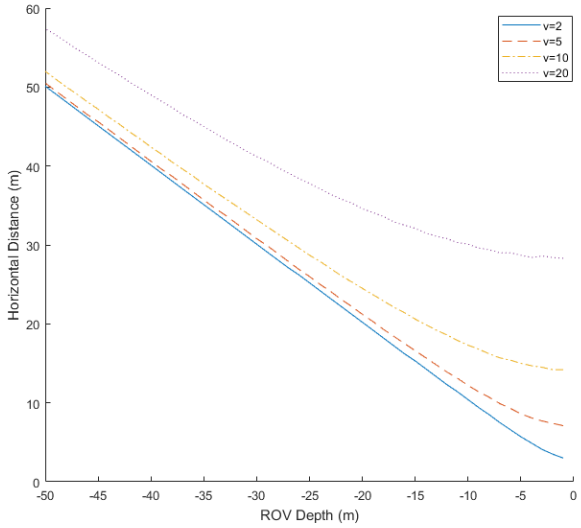

Figure 4.7: Horizontal distance in function of ROV depth for different speeds of the ASV.

ranges and speed of the ASV are known. This position is the one where the determinant of the FIM within the range of the ASV is maximum.

These distances were calculated for different speeds of the ASV and are shown in figure 4.7. While most ASVs can't travel as fast as some of speeds shown in the graph, these are presented as a hypothetical scenario.

The maximum determinant of the information matrix for the first two measurements achievable in function of the ROV's depth for different speeds of the ASV is shown in figure 4.8.

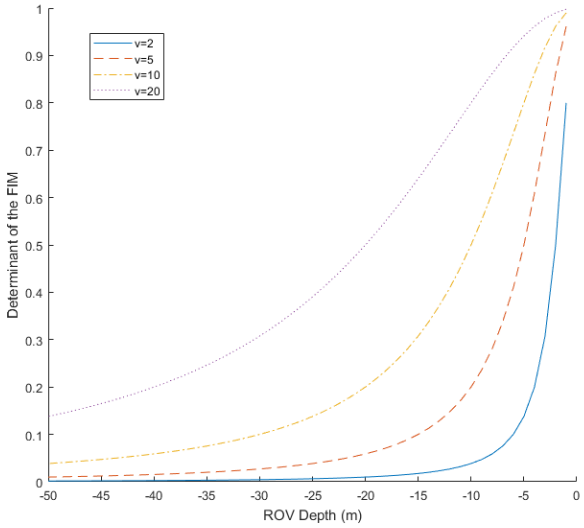

Figure 4.8: Maximum determinant of the FIM in function of ROV depth for different speeds of the ASV.

Using this information, the guidance algorithm was tested with the ROV stopped and moving according to the three different paths in figure 4.3 and the ASV in the optimal starting position shown in figure 4.7. The ASV was assumed to have a maximum velocity of 2 m/s.

The ROV's starting point in the horizontal plane was always (0, 0), and various initial depths were tested. An example of the paths of the ASV for each path of the ROV as well as the estimate error for each test is shown in figures 4.9 to 4.12.

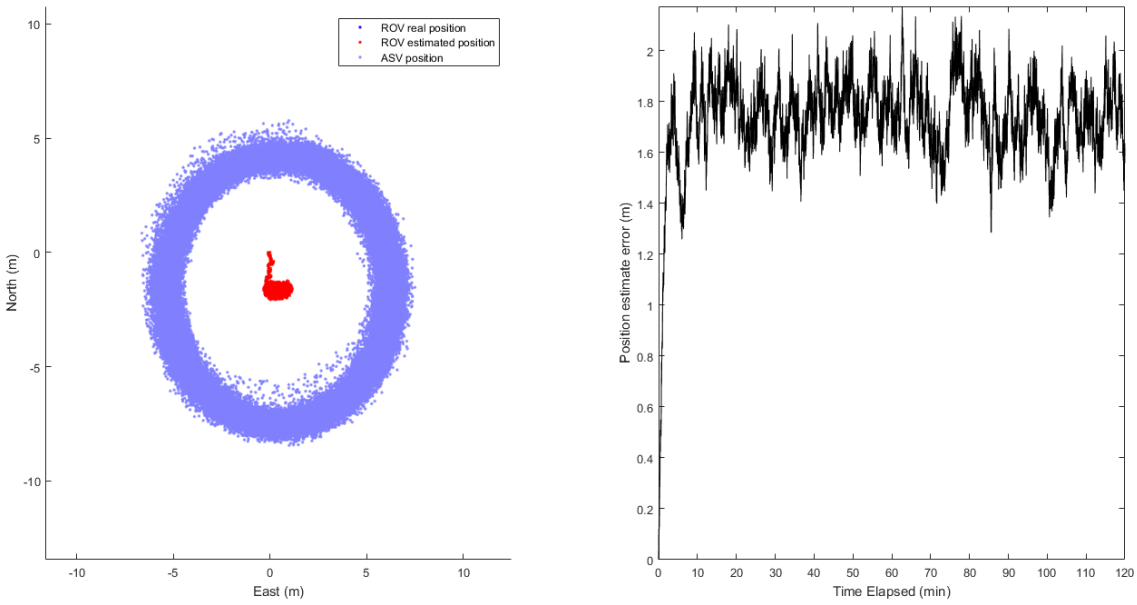

Figure 4.9: Simulation using Approach A with the ROV stopped at (0, 0, -5).

In table 4.1 the results of all the tests made using this approach for the guidance algorithm are shown.

Table 4.1: Results of testing approach A with the 4 ROV paths at different depths.

Depth	Stationary	Lawn Mower	Circular	Spiral
1m	$\bar{\varepsilon} = 0.810$ $\sigma_\varepsilon^2 = 0.021$	$\bar{\varepsilon} = 0.689$ $\sigma_\varepsilon^2 = 0.016$	$\bar{\varepsilon} = 0.575$ $\sigma_\varepsilon^2 = 0.063$	$\bar{\varepsilon} = 1.970$ $\sigma_\varepsilon^2 = 1.102$
5m	$\bar{\varepsilon} = 1,720$ $\sigma_\varepsilon^2 = 0.034$	$\bar{\varepsilon} = 1.362$ $\sigma_\varepsilon^2 = 0.043$	$\bar{\varepsilon} = 1.255$ $\sigma_\varepsilon^2 = 0.193$	$\bar{\varepsilon} = 2.016$ $\sigma_\varepsilon^2 = 1.080$
20m	$\bar{\varepsilon} = 1.820$ $\sigma_\varepsilon^2 = 0.124$	$\bar{\varepsilon} = 1.482$ $\sigma_\varepsilon^2 = 0.361$	$\bar{\varepsilon} = 1.488$ $\sigma_\varepsilon^2 = 0.407$	$\bar{\varepsilon} = 2.530$ $\sigma_\varepsilon^2 = 1.499$
50m	$\bar{\varepsilon} = 1.78$ $\sigma_\varepsilon^2 = 1.213$	$\bar{\varepsilon} = 2.309$ $\sigma_\varepsilon^2 = 0.647$	$\bar{\varepsilon} = 2.135$ $\sigma_\varepsilon^2 = 0.945$	$\bar{\varepsilon} = 3.542$ $\sigma_\varepsilon^2 = 2.228$

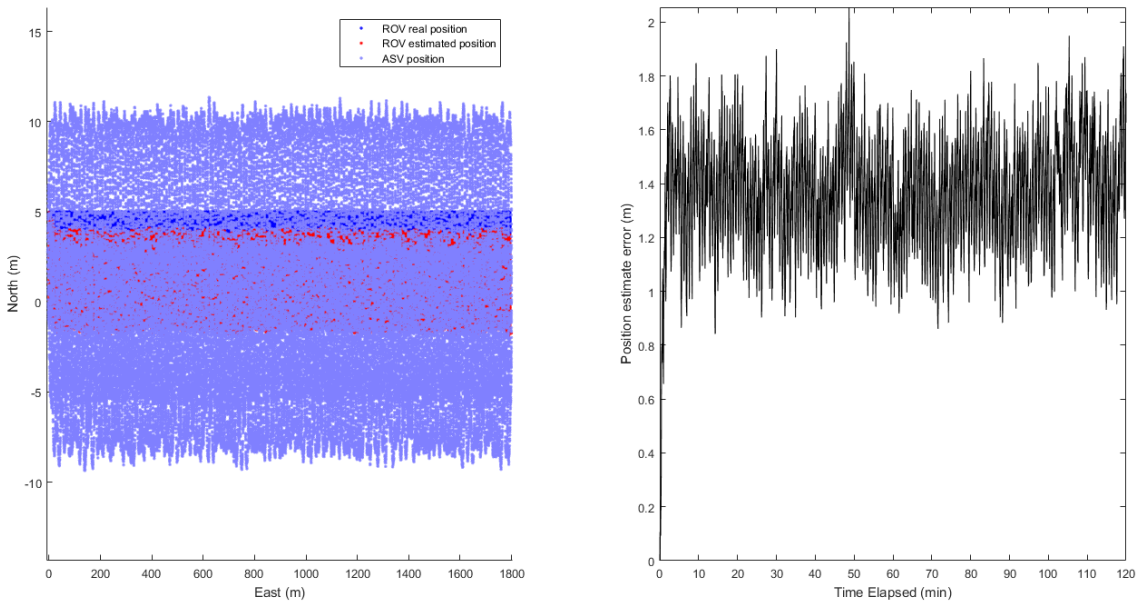

Figure 4.10: Simulation using Approach A with the ROV moving in the lawn mower pattern and starting at (0, 0, -5).

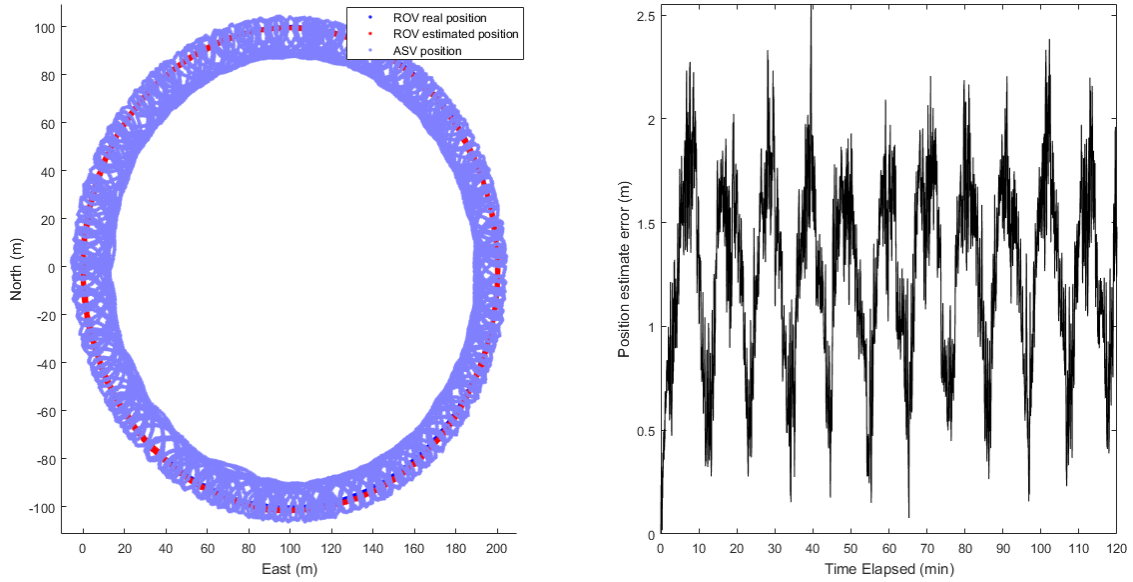

Figure 4.11: Simulation using Approach A with the ROV moving in a spiral and starting at (0, 0, -5).

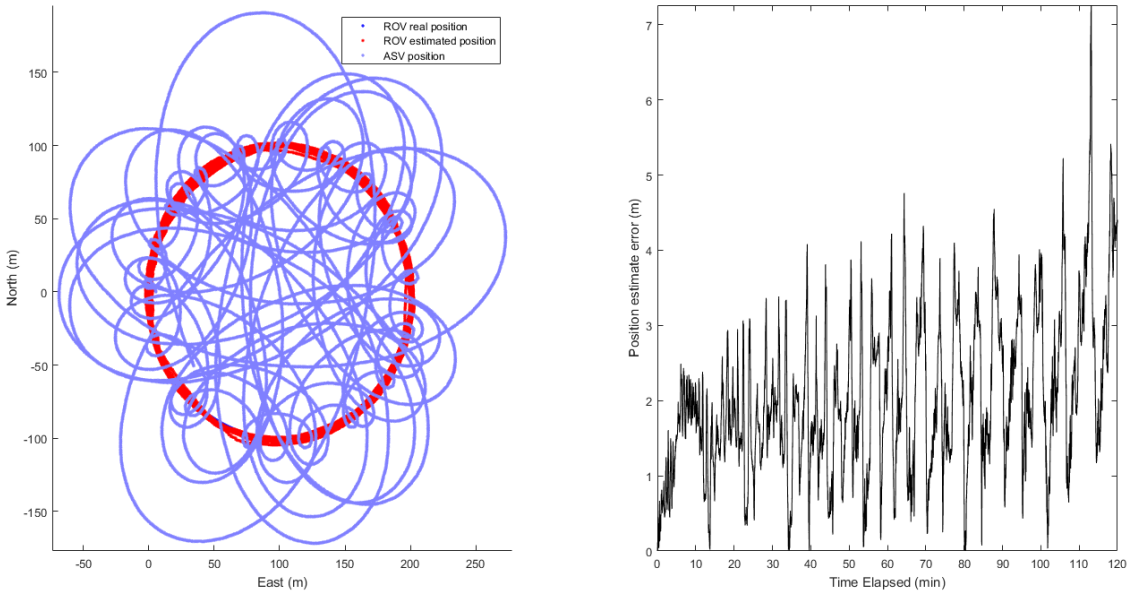

Figure 4.12: Simulation using Approach A with the ROV moving in a circle and starting at (0, 0, -5).

4.2.2 Approach B

The tests made for approach A were also made for approach B. It is considered that no information about the movement of the ROV is available in the beginning of the mission, so the method used for determining the initial position of the ASV was the same as the one used for approach A, meaning that the only difference between the tests was the guidance algorithm used.

The results of four of the simulations carried out with this approach are shown in figures 4.13 to 4.16.

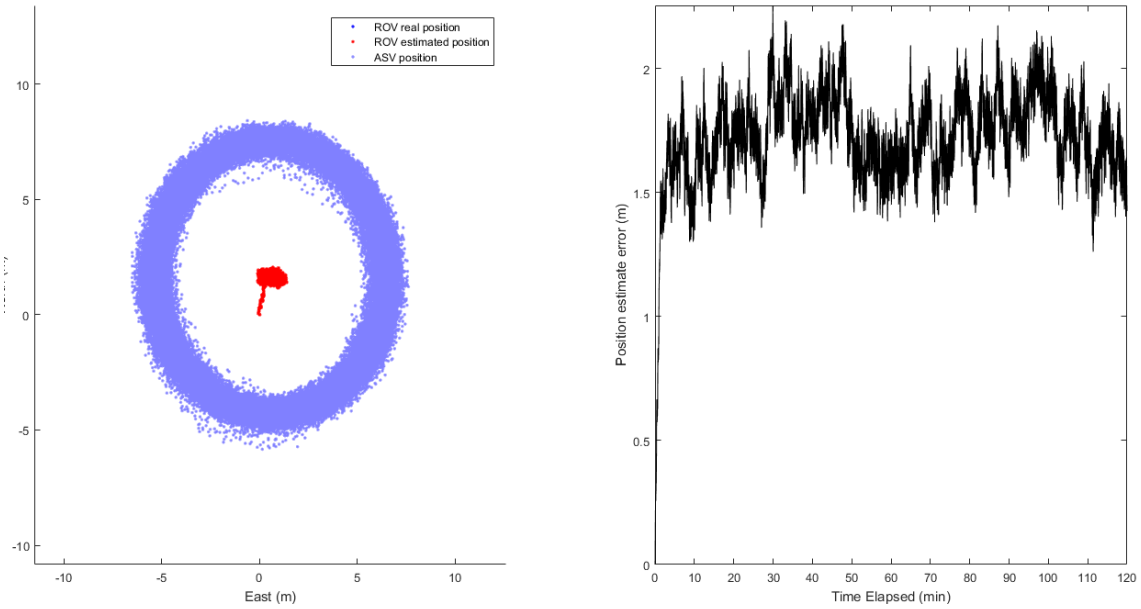

Figure 4.13: Simulation using Approach B with the ROV stopped at (0, 0, -5).

As mentioned in section 3.3.3, this approach includes the movement of the ROV in the guidance of the ASV, by including the estimated position of the ROV at the time the next signal will be sent. The estimated future position of the ROV was calculated under the assumption that its linear and angular speeds remain constant until the next range. In table 4.2 the results of all the tests made using this approach for the guidance algorithm are shown.

Table 4.2: Results of testing approach B with the 4 ROV paths at different depths.

Depth	Stationary	Lawn Mower	Circular	Spiral
1m	$\bar{\varepsilon} = 0.690$ $\sigma_\varepsilon^2 = 0.102$	$\bar{\varepsilon} = 0.659$ $\sigma_\varepsilon^2 = 0.014$	$\bar{\varepsilon} = 0.537$ $\sigma_\varepsilon^2 = 0.050$	$\bar{\varepsilon} = 4.309$ $\sigma_\varepsilon^2 = 6.842$
5m	$\bar{\varepsilon} = 1,730$ $\sigma_\varepsilon^2 = 0.039$	$\bar{\varepsilon} = 1.415$ $\sigma_\varepsilon^2 = 0.043$	$\bar{\varepsilon} = 1.170$ $\sigma_\varepsilon^2 = 0.073$	$\bar{\varepsilon} = 4.933$ $\sigma_\varepsilon^2 = 6.907$
20m	$\bar{\varepsilon} = 1.817$ $\sigma_\varepsilon^2 = 0.134$	$\bar{\varepsilon} = 1.479$ $\sigma_\varepsilon^2 = 0.207$	$\bar{\varepsilon} = 5.637$ $\sigma_\varepsilon^2 = 4.168$	$\bar{\varepsilon} = 5.041$ $\sigma_\varepsilon^2 = 4.883$
50m	$\bar{\varepsilon} = 1.568$ $\sigma_\varepsilon^2 = 1.236$	$\bar{\varepsilon} = 2.150$ $\sigma_\varepsilon^2 = 0.478$	$\bar{\varepsilon} = 5.074$ $\sigma_\varepsilon^2 = 4.703$	$\bar{\varepsilon} = 5.375$ $\sigma_\varepsilon^2 = 3.726$

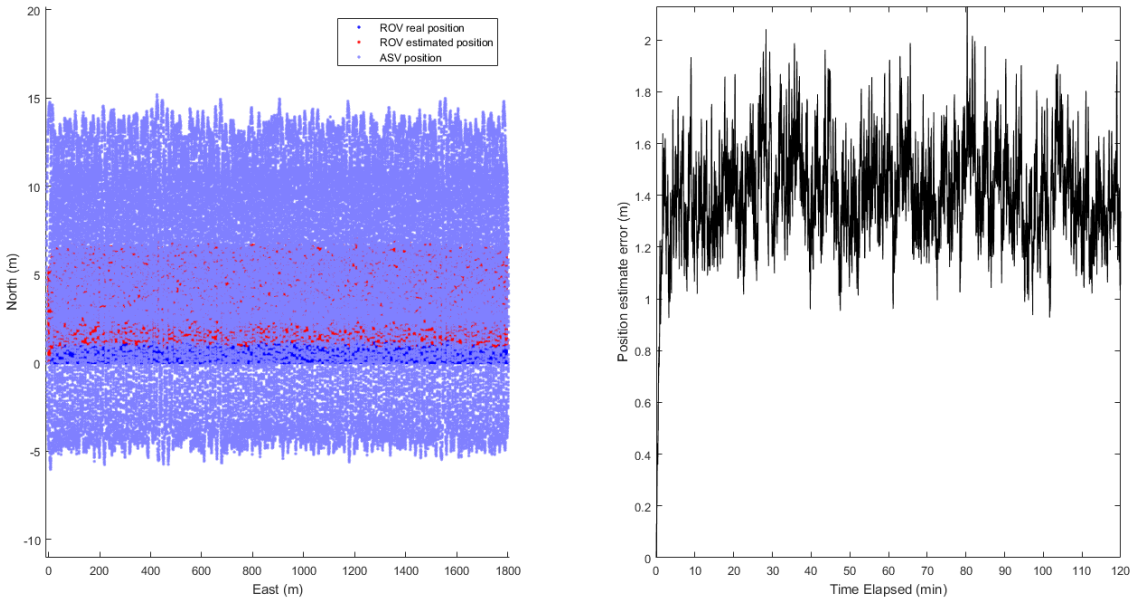

Figure 4.14: Simulation using Approach B with the ROV moving in the lawn mower pattern and starting at (0, 0, -5).

Comparing the results of the test made using both approaches, it can be stated that, despite approach B having a slightly better performance that approach A in some cases, there are cases where the error and variance of the estimation is significantly higher.

One possible explanation for this occurrence is the method for obtaining the future position, since the assumption that the ROV will maintain its course until the next range may not be true and that the information about the ROV's movement is obtained by sensors and therefore prone to error.

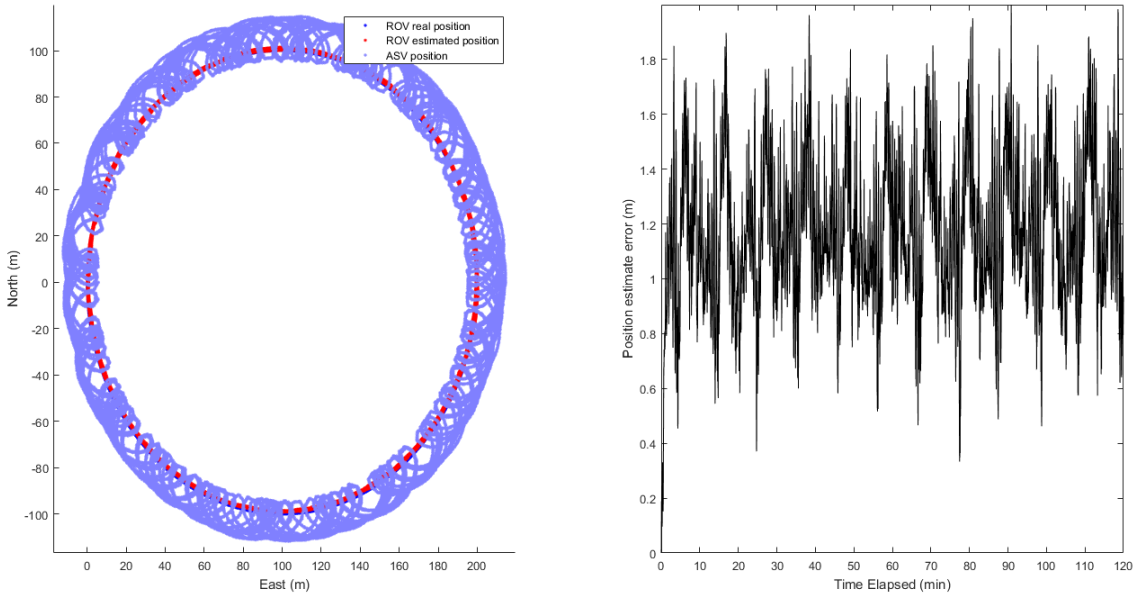

Figure 4.15: Simulation using Approach B with the ROV moving in a circle and starting at (0, 0, -5).

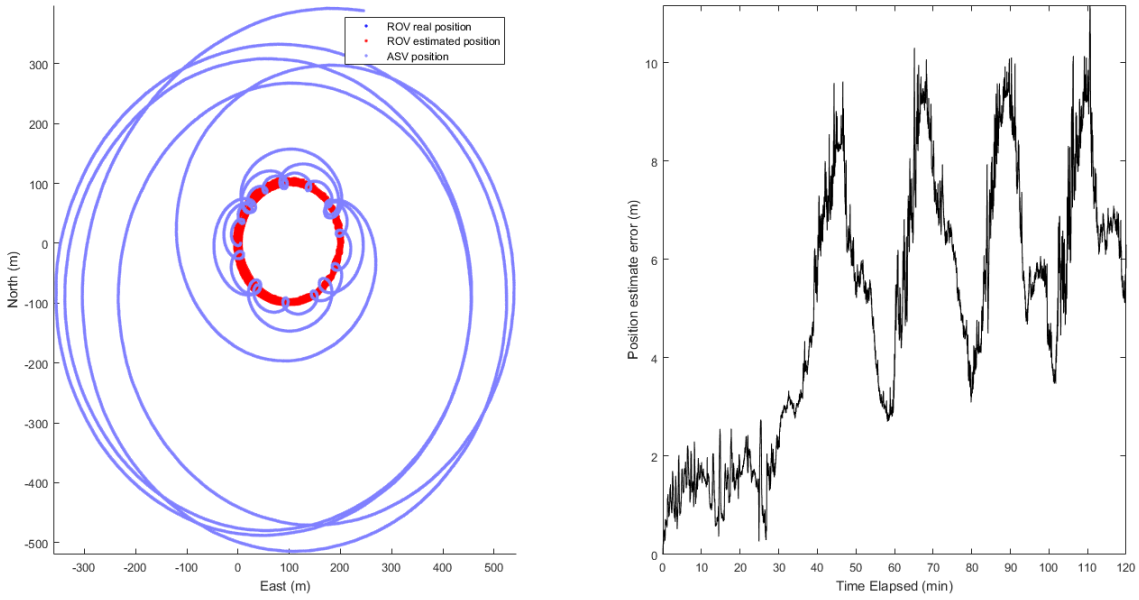

Figure 4.16: Simulation using Approach B with the ROV moving in a spiral and starting at (0, 0, -5).

Chapter 5

Conclusions and Future Work

In this thesis, a guidance algorithm for an ASV to be used as a navigation aid for a UUV was developed. This work is based on treating the proposed guidance problem as a sensor-target placement geometry, which was resolved with two different metrics based on the analysis of the Fisher Information Matrix. Furthermore, the metrics used for guidance of the ASV also provide relevant information about the optimal initial positioning of the ASV relatively to the ROV.

The results of the performed tests indicate that the estimation error when estimating the position of a UUV using DR and a single moving beacon depend on the operating depth of the UUV and the maximum velocity of the ASV.

When analyzing the results of the performed tests, it can be verified that the positioning errors are low when compared to other similar works. However that direct comparison should only be taken as an indicator of the relevance of this approach to the problem, because of the simplicity of the simulation environment and the assumptions made about the reaching set of the surface vehicle.

Overall, it is possible to conclude that the the FIM is an appropriate tool for use in the guidance of a CNA surface vehicle.

In order to develop a full localization system based on this work, it is advised that a kinetics model for the vehicles is included in the simulation environment, as well as real sensor data, in order to improve the simulation environment by making it more similar to a real situation. Furthermore, a more realistic model of the ASV's reaching set should be used in the guidance algorithm.

Appendix A

EKF equations

$$X(k+1) = \begin{bmatrix} N(k+1) \\ E(k+1) \\ D(k+1) \\ \theta(k+1) \\ \phi(k+1) \\ \psi(k+1) \end{bmatrix} = f(X(k), \nu(k)) + \mathcal{N}(0, Q(k)) \tag{A.1}$$

$$f(X(k), \nu(k)) = X(k) + \Delta X(k) \tag{A.2}$$

$$\Delta X(k) = \Delta t \cdot J \cdot \nu = \begin{bmatrix} c(\psi)c(\theta) & c(\psi)s(\theta)s(\phi) - s(\psi)c(\phi) & s(\psi)s(\phi) + c(\psi)c(\phi)s(\theta) & 0 & 0 & 0 \\ s(\psi)c(\theta) & c(\psi)c(\phi) + s(\phi)s(\theta)s(\psi) & s(\theta)s(\psi)c(\phi) - c(\psi)s(\phi) & 0 & 0 & 0 \\ -s(\theta) & c(\theta)s(\phi) & -(\theta)c(\phi) & 0 & 0 & 0 \\ 0 & 0 & 0 & 1 & s(\phi)t(\theta) & c(\phi)t(\theta) \\ 0 & 0 & 0 & 0 & c(\phi) & -s(\phi) \\ 0 & 0 & 0 & 0 & \frac{s(\phi)}{c(\theta)} & \frac{c(\phi)}{c(\theta)} \end{bmatrix} \cdot \begin{bmatrix} u \\ v \\ w \\ p \\ q \\ r \end{bmatrix} \tag{A.3}$$

$$\Delta X(k) = \Delta t \cdot \begin{bmatrix} u(k) \cdot c(\psi(k))c(\theta(k-1)) + v(k) \cdot (c(\psi(k-1))s(\theta(k-1))s(\phi(k-1)) - s(\psi(k-1))c(\phi(k-1))) + w(k) \cdot (s(\psi(k-1))s(\phi(k-1)) + c(\psi(k-1))c(\phi(k-1))s(\theta(k-1))) \\ u(k) \cdot s(\psi(k-1))c(\theta(k-1)) + v(k) \cdot (c(\psi(k-1))c(\phi(k-1)) + s(\phi(k-1))s(\theta(k-1))s(\psi(k-1))) + w(k) \cdot (s(\theta(k-1))s(\psi(k-1))c(\phi(k-1)) - c(\psi(k-1))s(\phi(k-1))) \\ -u(k) \cdot s(\theta(k-1)) + v(k) \cdot c(\theta(k-1))s(\phi(k-1)) - w(k) \cdot c(\theta(k-1))c(\phi(k-1)) \\ p(k) \cdot + q(k) \cdot s(\phi(k-1))t(\theta(k-1)) + r(k) \cdot c(\phi(k-1))t(\theta(k-1)) \\ q(k) \cdot c(\phi(k-1)) - r(k) \cdot s(\phi(k-1)) \\ q(k) \cdot \frac{s(\phi(k-1))}{c(\theta(k-1))} + r(k) \cdot \frac{c(\phi(k-1))}{c(\theta(k-1))} \end{bmatrix} \tag{A.4}$$

$$\nabla_X f(X(k), \nu(k)) = \begin{bmatrix} \frac{\partial N(k+1)}{\partial N(k)} & \frac{\partial N(k+1)}{\partial E(k)} & \frac{\partial N(k+1)}{\partial D(k)} & \frac{\partial N(k+1)}{\partial \phi(k)} & \frac{\partial N(k+1)}{\partial \theta(k)} & \frac{\partial N(k+1)}{\partial \psi(k)} \\ \frac{\partial E(k+1)}{\partial N(k)} & \frac{\partial E(k+1)}{\partial E(k)} & \frac{\partial E(k+1)}{\partial D(k)} & \frac{\partial E(k+1)}{\partial \phi(k)} & \frac{\partial E(k+1)}{\partial \theta(k)} & \frac{\partial E(k+1)}{\partial \psi(k)} \\ \frac{\partial D(k+1)}{\partial N(k)} & \frac{\partial D(k+1)}{\partial E(k)} & \frac{\partial D(k+1)}{\partial D(k)} & \frac{\partial D(k+1)}{\partial \phi(k)} & \frac{\partial D(k+1)}{\partial \theta(k)} & \frac{\partial D(k+1)}{\partial \psi(k)} \\ \frac{\partial \phi(k+1)}{\partial N(k)} & \frac{\partial \phi(k+1)}{\partial E(k)} & \frac{\partial \phi(k+1)}{\partial D(k)} & \frac{\partial \phi(k+1)}{\partial \phi(k))} & \frac{\partial \phi(k+1)}{\partial \theta(k)} & \frac{\partial \phi(k+1)}{\partial \psi(k)} \\ \frac{\partial \theta(k+1)}{\partial N(k)} & \frac{\partial \theta(k+1)}{\partial E(k)} & \frac{\partial \theta(k+1)}{\partial D(k)} & \frac{\partial \theta(k+1)}{\partial \phi(k)} & \frac{\partial \theta(k+1)}{\partial \theta(k)} & \frac{\partial \theta(k+1)}{\partial \psi(k)} \\ \frac{\partial \psi(k+1)}{\partial N(k)} & \frac{\partial \psi(k+1)}{\partial E(k))} & \frac{\partial \psi(k+1)}{\partial D(k)} & \frac{\partial \psi(k+1)}{\partial \phi(k)} & \frac{\partial \psi(k+1)}{\partial \theta(k)} & \frac{\partial \psi(k+1)}{\partial \psi(k)} \end{bmatrix} \tag{A.5}$$

$$
\begin{aligned}
\frac{\partial N(k+1)}{\partial N(k)} &= 1 \\
\frac{\partial N(k+1)}{\partial E(k)} &= 0 \\
\frac{\partial N(k+1)}{\partial D(k)} &= 0 \\
\frac{\partial N(k+1)}{\partial \phi(k)} &= \Delta t\, p(k)(-u(k)s(\theta(k))c(\psi(k)) + v(k)c(\theta(k))c(\psi(k))s(\phi(k)) + w(k)c(\theta(k))c(\psi(k))c(\phi(k))) \\
\frac{\partial N(k+1)}{\partial \theta(k)} &= \Delta t\, q(k)(v(k)(s(\theta(k))c(\psi(k))c(\phi(k)) + s(\psi(k))s(\phi(k))) + w(k)p(k)(s(\psi(k))c(\phi(k)) - s(\theta(k))c(\psi(k))s(\phi(k)))) \\
\frac{\partial N(k+1)}{\partial \psi(k)} &= \Delta t\, r(k)(-u(k)c(\theta(k))s(\psi(k)) + v(k)(c(\psi(k))(-c(\phi(k))) - s(\theta(k))s(\psi(k))s(\phi(k))) + w(k)(c(\psi(k))s(\phi(k)) - s(\theta(k))s(\psi(k))c(\phi(k)))) \\
\frac{\partial E(k+1)}{\partial N(k)} &= 0 \\
\frac{\partial E(k+1)}{\partial E(k)} &= 1 \\
\frac{\partial E(k+1)}{\partial D(k)} &= 0 \\
\frac{\partial E(k+1)}{\partial \phi(k)} &= \Delta t\, p(k)(-u(k)s(\theta(k))s(\psi(k)) + v(k)c(\theta(k))s(\psi(k))s(\phi(k)) + w(k)c(\theta(k))s(\psi(k))c(\phi(k))) \\
\frac{\partial E(k+1)}{\partial \theta(k)} &= \Delta t\, q(k)(v(k)(s(\theta(k))s(\psi(k))c(\phi(k)) - c(\psi(k))s(\phi(k))) + w(k)(c(\psi(k))(-c(\phi(k))) - s(\theta(k))s(\psi(k))s(\phi(k)))) \\
\frac{\partial E(k+1)}{\partial \psi(k)} &= \Delta t\, r(k)(u(k)c(\theta(k))c(\psi(k)) + v(k)(s(\theta(k))c(\psi(k))s(\phi(k)) - s(\psi(k))c(\phi(k))) + w(k)(s(\theta(k))c(\psi(k))c(\phi(k)) + s(\psi(k))s(\phi(k)))) \\
\frac{\partial D(k+1)}{\partial N(k)} &= 0 \\
\frac{\partial D(k+1)}{\partial E(k)} &= 0 \\
\frac{\partial D(k+1)}{\partial D(k)} &= 1 \\
\frac{\partial D(k+1)}{\partial \phi(k)} &= \Delta t\, p(k)(-u(k)c(\theta(k)) - v(k)s(\theta(k))s(\phi(k)) + w(k)s(\theta(k))c(\phi(k))) \\
\frac{\partial D(k+1)}{\partial \theta(k)} &= \Delta t\, q(k)(c(\theta(k))(v(k)c(\phi(k)) + w(k)s(\phi(k)))) \\
\frac{\partial D(k+1)}{\partial \psi(k)} &= 0 \\
\frac{\partial \phi(k+1)}{\partial N(k)} &= 0 \\
\frac{\partial \phi(k+1)}{\partial E(k)} &= 0 \\
\frac{\partial \phi(k+1)}{\partial D(k)} &= 0 \\
\frac{\partial \phi(k+1)}{\partial \phi(k)} &= 1 + \Delta t\, p(k)(q(k)sec^2(\theta(k))s(\phi(k)) + r(k)sec^2(\theta(k))c(\phi(k))) \\
\frac{\partial \phi(k+1)}{\partial \theta(k)} &= \Delta t\, q(k)(q(k)t(\theta(k))c(\phi(k)) - r(k)t(\theta(k))s(\phi(k))) \\
\frac{\partial \phi(k+1)}{\partial \psi(k)} &= 0 \\
\frac{\partial \theta(k+1)}{\partial N(k)} &= 0 \\
\frac{\partial \theta(k+1)}{\partial E(k)} &= 0 \\
\frac{\partial \theta(k+1)}{\partial D(k)} &= 0 \\
\frac{\partial \theta(k+1)}{\partial \phi(k)} &= 0 \\
\frac{\partial \theta(k+1)}{\partial \phi(k)} &= 1 + \Delta t\, q(k)(-q(k)s(\phi(k)) - r(k)c(\phi(k))) \\
\frac{\partial \theta(k+1)}{\partial \psi(k)} &= 0 \\
\frac{\partial \psi(k+1)}{\partial N(k)} &= 0 \\
\frac{\partial \psi(k+1)}{\partial E(k)} &= 0 \\
\frac{\partial \psi(k+1)}{\partial D(k)} &= 0 \\
\frac{\partial \psi(k+1)}{\partial \phi(k)} &= \Delta t\, p(k)t(\theta(k))sec(\theta(k))(q(k)s(\phi(k)) + r(k)c(\phi(k))) \\
\frac{\partial \psi(k+1)}{\partial \theta(k)} &= \Delta t\, q(k)sec(\theta(k))(q(k)c(\phi(k)) - r(k)s(\phi(k))) \\
\frac{\partial \psi(k+1)}{\partial \psi(k)} &= 1
\end{aligned}
\tag{A.6}
$$

References

[1] Brian Bingham. Navigating Autonomous Underwater Vehicles. *Underwater Vehicles*, pages 33–50, 2009.

[2] Liam Paull, Sajad Saeedi, Mae Seto, and Howard Li. AUV navigation and localization: A review, 2014. doi:10.1109/JOE.2013.2278891.

[3] Hwee Pink Tan, Roee Diamant, Winston K.G. Seah, and Marc Waldmeyer. A survey of techniques and challenges in underwater localization, 2011. doi:10.1016/j.oceaneng.2011.07.017.

[4] Bruno Ferreira, Aníbal Matos, and Nuno Cruz. Single beacon navigation: Localization and control of the MARES AUV. In *MTS/IEEE Seattle, OCEANS 2010*, 2010. doi:10.1109/OCEANS.2010.5664518.

[5] Pedro Batista, Carlos Silvestre, and Paulo Oliveira. Single range aided navigation and source localization: Observability and filter design. *Systems and Control Letters*, 2011. doi:10.1016/j.sysconle.2011.05.004.

[6] Mandar Chitre. Path planning for cooperative underwater range-only navigation using a single beacon. In *IEEE 2010 International Conference on Autonomous and Intelligent Systems, AIS 2010*, 2010. doi:10.1109/AIS.2010.5547044.

[7] Alexander Bahr, John J. Leonard, and Maurice F. Fallon. Cooperative localization for autonomous underwater vehicles. *International Journal of Robotics Research*, 28(6):714–728, 2009. doi:10.1177/0278364908100561.

[8] Maurice F. Fallon, Georgios Papadopoulos, John J. Leonard, and Nicholas M. Patrikalakis. Cooperative AUV navigation using a single maneuvering surface craft. *International Journal of Robotics Research*, 29(12):1461–1474, 2010. doi:10.1177/0278364910380760.

[9] Daniel Viegas, Pedro Batista, Paulo Oliveira, and Carlos Silvestre. Position and velocity filters for asc/i-auv tandems based on single range measurements. *Journal of Intelligent and Robotic Systems: Theory and Applications*, 2014. doi:10.1007/s10846-013-9876-9.

[10] Yew Teck Tan, Rui Gao, and Mandar Chitre. Cooperative path planning for range-only localization using a single moving beacon. *IEEE Journal of Oceanic Engineering*, 2014. doi:10.1109/JOE.2013.2296361.

[11] I. Masmitja, P.J. Bouvet, S. Gomariz, J. Aguzzi, and J. del Rio. Underwater mobile target tracking with particle filter using an autonomous vehicle. *OCEANS 2017 - Aberdeen*, 2017. doi:10.1109/OCEANSE.2017.8084692.

[12] Thor I. Fossen. *Handbook of Marine Craft Hydrodynamics and Motion Control*. 2011. doi:10.1002/9781119994138.

[13] Sebastian Thrun. *Probabilistic robotics*. 2005.

[14] Sarah E. Webster, Louis L. Whitcomb, and Ryan M. Eustice. Advances in decentralized single-beacon acoustic navigation for underwater vehicles: Theory and simulation. In *2010 IEEE/OES Autonomous Underwater Vehicles, AUV 2010*, 2010. doi:10.1109/AUV.2010.5779677.

[15] Nicholas R. Rypkema, Erin M. Fischell, and Henrik Schmidt. One-way travel-time inverted ultra-short baseline localization for low-cost autonomous underwater vehicles. *Proceedings - IEEE International Conference on Robotics and Automation*, pages 4920–4926, 2017. doi:10.1109/ICRA.2017.7989570.

[16] Sajad Saeedi, Mae Seto, and Howard Li. Fast Monte Carlo localization of AUV using acoustic range measurement. *Canadian Conference on Electrical and Computer Engineering*, 2015-June(June):326–331, 2015. doi:10.1109/CCECE.2015.7129297.

[17] Fedor S. Dubrovin and Alexander Ph Scherbatyuk. About accuracy estimation of AUV single-beacon mobile navigation using ASV, equipped with DGPS. *OCEANS 2016 - Shanghai*, pages 0–3, 2016. doi:10.1109/OCEANSAP.2016.7485435.

[18] I N Burdinsky and S A Otcheskii. Observation error estimation in case of an AUV using a single beacon acoustic positioning system. In *2017 24th Saint Petersburg International Conference on Integrated Navigation Systems, ICINS 2017 - Proceedings*, 2017. doi:10.23919/ICINS.2017.7995596.

[19] N Crasta, David Moreno-Salinas, Behzad Bayat, Antonio M Pascoal, and J Aranda. Range-based underwater target localization using an autonomous surface vehicle: Observability analysis. 2018.

[20] Adrian N. Bishop, Bariş Fidan, Brian D.O. Anderson, Kutluyil Doğançay, and Pubudu N. Pathirana. Optimality analysis of sensor-target localization geometries. *Automatica*, 2010. doi:10.1016/j.automatica.2009.12.003.

[21] Bruno M Ferreira, Aníbal C Matos, Helder S Campos, and Nuno A Cruz. Localization of a sound source: optimal positioning of sensors carried on autonomous surface vehicles.